Search for new physics with jets and missing transverse momentum in pp collisions at s√=7 TeV

Journal Article

Author(s):
CMS Collaboration; Chatrchyan, Serguei; Bäni, Lukas; Bortignon, Pierluigi; Caminada, Lea; Chanon, Nicolas; Chen, Zhiling; Cittolin, Sergio; Dissertori, Günther; Dittmar, Michael; Eugster, Jürg; Freudenreich, Klaus; Grab, Christoph; Hintz, Wieland; Lecomte, Pierre; Lustermann, Werner; Marchica, Carmelo; Martinez Ruiz del Arbol, Pablo; Milenovic, Predrag; Moortgat, Filip; Nägeli, Christoph; Nef, Pascal; Nessi-Tedaldi, Francesca; Pape, Luc; Pauss, Felicitas; Punz, Thomas; Rizzi, Andrea; Ronga, Frédéric J.; Rossini, Marco; Sala, Leonardo; Sanchez, Ann-Karin; Sawley, Marie-Christine; Stieger, Benjamin; Tauscher, Ludwig; Thea, Alessandro; Theofilatos, Konstantinos; Treille, Daniel; Urscheler, Christina; Wallny, Rainer; Weber, Marc; Wehrli, Lukas; Weng, Johanna; et al.

Search for new physics with jets and missing transverse momentum in pp collisions at $\sqrt{s} = 7$ TeV

The CMS Collaboration

ABSTRACT: A search for new physics is presented based on an event signature of at least three jets accompanied by large missing transverse momentum, using a data sample corresponding to an integrated luminosity of $36\,\mathrm{pb}^{-1}$ collected in proton-proton collisions at $\sqrt{s} = 7\,\mathrm{TeV}$ with the CMS detector at the LHC. No excess of events is observed above the expected standard model backgrounds, which are all estimated from the data. Exclusion limits are presented for the constrained minimal supersymmetric extension of the standard model. Cross section limits are also presented using simplified models with new particles decaying to an undetected particle and one or two jets.

Contents

1 Introduction

Several theories beyond the standard model (SM) of particle physics address the gauge hierarchy problem and other shortcomings of the SM by introducing a spectrum of new particles that are partners of the SM particles [1–3]. These new particles may include neutral, stable, and weakly interacting particles that are good dark-matter candidates. The identity and properties of the fundamental particle(s) that make up dark matter are two of the most important unsolved problems in particle physics and cosmology. The energy density of dark matter is approximately five times larger than for the normal baryonic matter that corresponds to the luminous portion of the universe. A review on dark matter can be found in ref. [4].

Many dark-matter candidates are stable as a result of a conserved quantity. In supersymmetry (SUSY) this quantity is R parity, and its conservation requires all SUSY particles to be produced in pairs and the lightest SUSY particle (LSP) to be stable. Coloured SUSY particles can be pair-produced copiously at the Large Hadron Collider (LHC). These particles will decay directly into SM particles and an LSP or via intermediate colour-singlet states that ultimately decay into an LSP, resulting in a large amount of energy deposited in the detector. The LSP will pass through the detector without interacting, carrying away a substantial amount of energy and creating an imbalance in the measured transverse momentum (p_T).

Experiments at the Tevatron [5–7], SPS [8, 9], LEP [10–13], and HERA colliders [14, 15] have performed extensive searches for SUSY and set lower limits on the masses of SUSY particles. At the LHC, the CMS Collaboration has previously published limits in the all-hadronic channel based on a search using the α_T [16] kinematic variable [17]. The ATLAS Collaboration has also published limits from a missing transverse momentum and multijet search [18].

In this paper, results are presented from a search for large missing transverse momentum in multijet events produced in pp collisions at a centre-of-mass-energy of 7 TeV, using a data sample collected with the CMS detector at the LHC in 2010, corresponding to an integrated luminosity of 36 pb^{-1}. The results of the search are presented in the context of the constrained minimal supersymmetric extension of the standard model (CMSSM) [19–22], and in the more general context of simplified models [23–26]. These latter models are designed to characterize experimental data in terms of a small number of particles whose masses and decay branching fractions are allowed to vary freely. The results are independent of any more complete theory that addresses the deeper problems of particle physics, yet they can be translated into any such desired framework.

This search is complementary to the CMS analysis [17] that used the kinematic variable α_T as the search variable in events with at least two jets. That variable is very effective in suppressing the QCD multijet background but with some loss of signal acceptance. In contrast, this search only selects events with ≥ 3 jets, and the missing and visible transverse momentum sums are used as search variables for an inclusive selection with a higher signal acceptance.

The main backgrounds in this analysis are: (a) an irreducible background from Z+jets events, with the Z boson decaying to $\nu\bar{\nu}$, denoted as Z($\nu\bar{\nu}$)+jets; (b) W+jets and $t\bar{t}$ events, with either the directly-produced W boson or one of the W bosons from the top-quark decays going directly or via a τ to an e or μ that is lost, or going to a τ that decays hadronically. In all these cases, one or more neutrinos provide a genuine source of missing transverse momentum; and (c) QCD multijet events with large missing transverse momentum from leptonic decays of heavy-flavour hadrons inside the jets, jet energy mismeasurement, or instrumental noise and non-functioning detector components. The relative contributions of these three categories of backgrounds depend on the event selection.

This paper is organized as follows. The CMS detector and event reconstruction are described in section 2. In section 3, the event selection criteria are presented. The backgrounds to this search are directly determined from the data, in some cases with novel

techniques which are being applied here for the first time. In section 4, the irreducible $Z(\nu\bar{\nu})$+jets background is estimated from γ+jets events, and alternative Z and W control samples are studied. The background from W+jets and $t\bar{t}$ where a lepton is either lost or is a hadronically decaying tau lepton is estimated from μ+jets events by ignoring or replacing the muon, as discussed in section 5. The QCD multijet kinematics are predicted using measured jet resolution functions to smear events obtained by a procedure that produces well-balanced events out of inclusive multijet data, as discussed in section 6. As a cross-check, the correlation between the transverse missing momentum vector and the angular distance between that vector and the closest leading jet is used to predict the tail of the missing-momentum distribution. In section 7, the interpretation of the observed data is presented.

2 The CMS detector and event reconstruction

The central feature of the CMS apparatus is a superconducting solenoid 13 m in length and 6 m in diameter, which provides an axial magnetic field of 3.8 T. The bore of the solenoid is instrumented with various particle detection systems. The steel return yoke outside the solenoid is in turn instrumented with gas detectors which are used to identify muons. Charged particle trajectories are measured by the silicon pixel and strip tracker, covering $0 < \phi < 2\pi$ in azimuth and $|\eta| < 2.5$, where the pseudorapidity η is defined as $\eta = -\ln[\tan(\theta/2)]$, with θ being the polar angle of the particle's momentum with respect to the counterclockwise beam direction. A lead-tungstate crystal electromagnetic calorimeter (ECAL) and a brass/scintillator hadronic calorimeter (HCAL) surround the tracking volume and cover the region $|\eta| < 3$. Quartz/steel forward hadron calorimeters extend the coverage to $|\eta| \leq 5$. The detector is nearly hermetic, allowing for momentum balance measurements in the plane transverse to the beam directions. A detailed description of the CMS detector can be found elsewhere [27].

All physics objects are reconstructed with a particle-flow technique [28]. This algorithm identifies and reconstructs individually the particles produced in the collision, namely charged and neutral hadrons, photons, muons, and electrons, by combining the information from the tracking system, the calorimeters, and the muon system. All these particles are clustered into jets using the anti-k_T algorithm with a distance parameter of 0.5 [29] from FASTJET [30]. Jet energies are corrected for the non-linear calorimeter response using calibration factors derived from simulation, and, for jets in data, an additional residual energy correction derived from data is applied [31]. As the average number of additional pileup interactions during the LHC 2010 data taking is roughly between two and three, no subtraction of the pileup energy deposits is performed.

3 Sample selection

The event selection for this search aims to be inclusive, such that it can detect new physics from any model yielding a high-multiplicity hadronic final state with missing transverse momentum. Therefore, the observables of central interest in the search are chosen to

be the magnitude of the missing transverse momentum $\not{H}_\mathrm{T}$ calculated from jets, and the scalar sum of the jet transverse momenta H_T. The choice of these observables and the applied background suppression cuts aim for a minimal kinematic bias in the search for new physics signals. This facilitates the characterization of new physics in the case of a discovery. Furthermore, the selection is chosen to be efficient for models containing new particles with sufficiently small mass and thus sizeable production yield for the integrated luminosity used in this search. In this section, the event selection is described, based on the above considerations.

3.1 Trigger selection and cleaning of the data sample

The data used in this analysis were collected with triggers based on the quantity $H_\mathrm{T}^\mathrm{trig}$, defined as the scalar sum of the transverse momenta of reconstructed calorimeter jets (without response corrections) having $p_\mathrm{T} > 20\,\mathrm{GeV}$ and $|\eta| < 5$. The $H_\mathrm{T}^\mathrm{trig}$ threshold varied between 100 and $150\,\mathrm{GeV}$ as the instantaneous luminosity of the LHC increased. The H_T trigger has a high acceptance for low-mass hadronic, new-physics signatures, and it enables the simultaneous collection of several control samples used to estimate the backgrounds. The trigger efficiency as a function of the particle-flow-based H_T, defined below in section 3.2, was measured using data taken with a single-calorimeter-jet trigger. It was found to be close to 100% for H_T values above 300 GeV.

Ways to remove events with a poor $\not{H}_\mathrm{T}$ measurement were investigated using both simulation and data. Various sources of noise in the electromagnetic and hadronic calorimeters are rejected [32, 33]. Beam-related background events and displaced satellite collisions are removed by requiring a well-reconstructed primary vertex within the luminous region, applying a beam-halo veto [33], asking for a significant fraction of tracks in the event to be of high quality, and requiring the scalar sum of the transverse momenta of tracks associated with the primary vertex to be greater than 10% of the scalar sum of the transverse momenta of all jets within the tracker acceptance. Events are also rejected in which a significant amount of energy is determined to have been lost in the approximately 1% of non-functional crystals in the ECAL that are masked in reconstruction [32]. Such losses are identified either by exploiting the energy measured through a parallel readout path used for the online trigger, or by measuring the energy deposited around masked crystals when information from this parallel readout path is not available. The small inefficiency for signal events induced by this cleaning is discussed further in section 7.1.

3.2 Baseline and search event selections

The search selection starts from a loosely selected sample of candidate events. From this so-called baseline sample, tighter search selection criteria are then applied to obtain the final event sample. The baseline selection requirements are:

- At least three jets with $p_\mathrm{T} > 50\,\mathrm{GeV}$ and $|\eta| < 2.5$.

- $H_\mathrm{T} > 300\,\mathrm{GeV}$, with H_T defined as the scalar sum of the transverse momenta of all jets with $p_\mathrm{T} > 50\,\mathrm{GeV}$ and $|\eta| < 2.5$.

- $H̸_T > 150\,\text{GeV}$, with $H̸_T$ defined as the magnitude of the negative vector sum of the transverse momenta of all jets with $p_T > 30\,\text{GeV}$ and $|\eta| < 5$. This requirement suppresses the vast majority of the QCD multijet events.

- $|\Delta\phi(J_n, H̸_T)| > 0.5$, $n = 1, 2$ and $|\Delta\phi(J_3, H̸_T)| > 0.3$, where $\Delta\phi$ is the azimuthal angular difference between the jet axis J_n and the $H̸_T$ direction for the three highest-p_T jets in the event. This requirement rejects most of the QCD multijet events in which a single mismeasured jet yields a high-$H̸_T$ value.

- No isolated muons or electrons in the event. This requirement reduces the background from the leptonic final states of $t\bar{t}$ and W/Z+jets events. Muons and electrons are required to have $p_T > 10\,\text{GeV}$ and produce a good quality track that is matched to the primary vertex within $200\,\mu\text{m}$ transversely and $1\,\text{cm}$ longitudinally. They must also be loosely isolated, requiring a relative isolation variable to satisfy:

$$\left[\sum\nolimits^{\Delta R < 0.4} p_T{}^{\text{charged hadron}} + \sum\nolimits^{\Delta R < 0.4} p_T{}^{\text{neutral hadron}} + \sum\nolimits^{\Delta R < 0.4} p_T{}^{\text{photon}}\right] / p_T^{\text{lepton}} < 0.2,$$

  where $p_T{}^{\text{charged hadron}}$, $p_T{}^{\text{neutral hadron}}$, and $p_T{}^{\text{photon}}$ are, respectively, the momentum of charged hadrons, neutral hadrons, and photons in the event within a distance $\Delta R = 0.4$ in η–ϕ space of the lepton. Muons are required to have $|\eta| < 2.4$, whereas electrons must have $|\eta| < 2.5$, excluding the barrel-endcap transition region $1.44 < |\eta| < 1.57$.

Two search regions are chosen, based on the observables central to this inclusive jets-plus-missing-transverse-momentum search. The first selection, defining the high-$H̸_T$ search region, tightens the baseline cuts with a $H̸_T > 250\,\text{GeV}$ requirement, motivated by the search for a generic dark-matter candidate, which gives a large background rejection. The second selection adds a cut of $H_T > 500\,\text{GeV}$ to the baseline criteria, yielding the high-H_T search region, which is sensitive to the higher multiplicities from cascade decays of high-mass new-physics particles. Such cascades lead to more energy being transferred to visible particles and less to invisible ones.

3.3 Data-simulation comparison

Several Monte Carlo (MC) simulation samples are used, produced with a detailed CMS detector simulation based on GEANT4 [34]. Samples of QCD multijet, $t\bar{t}$, W/Z+jets, γ+jets, diboson, and single-top events were generated with the PYTHIA6 [35] and MADGRAPH [36] generators using the CTEQ6.1L [37] parton distribution functions. For the $t\bar{t}$ background an approximate next-to-next-to-leading-order (NNLO) cross section of $165\,\text{pb}$ [38] is used, while the cross sections for $W(\ell\nu)$+jets ($31\,300\,\text{pb}$) and $Z(\nu\bar{\nu})$+jets ($5\,769\,\text{pb}$) are derived from an NNLO calculation with FEWZ [39]. While already excluded [17], the LM1 CMSSM point [40] is used as a benchmark for new physics in this search. This point has a cross section of $6.5\,\text{pb}$ at NLO, calculated with PROSPINO [41]. It is defined to have a universal scalar mass $m_0 = 60\,\text{GeV}$, universal gaugino mass $m_{1/2} = 250\,\text{GeV}$, universal trilinear soft SUSY-breaking-parameter $A_0 = 0$, the ratio of the vacuum expectation values of the two

	Baseline no $\Delta\phi$ cuts no e/μ veto	Baseline no e/μ veto	Baseline selection	High-$\not{H}_T$ selection	High-H_T selection
LM1	71.2	60.4	45.0	31.3	33.8
QCD multijet	222.0	27.0	24.6	0.2	9.9
Z($\nu\bar{\nu}$)+jets	26.7	21.1	21.1	6.3	5.7
W($\ell\nu$)+jets	93.9	57.8	23.5	4.7	7.6
t$\bar{t}$	57.5	40.1	21.9	2.6	5.7
WW+WZ+ZZ+tW +Wγ+Zγ+Z/$\gamma^\star$	6.1	3.4	2.1	0.2	0.2
Total MC background	406	149	93	14	29
Data	482	180	111	15	40

Table 1. Event yields in data and simulated samples were produced for five different selection criteria. The latter are normalized to an integrated luminosity of $36\,\mathrm{pb}^{-1}$. All simulated samples were generated with the PYTHIA and MADGRAPH generators. The row labeled LM1 gives the expected yield for the benchmark supersymmetric model described in the text.

Higgs doublets $\tan\beta = 10$, and the sign of the Higgs mixing parameter sign(μ) positive. The squark and gluino masses for LM1 are respectively $559\,\mathrm{GeV}$ and $611\,\mathrm{GeV}$, and the LSP mass is $96\,\mathrm{GeV}$.

The event yields in the data and the simulated samples after two loose versions of the baseline selection, the baseline selection itself, and the two different search event selections are summarized in table 1, where the simulated event yields correspond to an integrated luminosity of $36\,\mathrm{pb}^{-1}$. The $\not{H}_T$ and H_T distributions for data and MC simulation are compared in figure 1 after the baseline selection. In the following sections, however, all the backgrounds in this search are estimated directly from data.

4   Z($\nu\bar{\nu}$)+jets background estimation

The production of a Z boson and jets, followed by the decay of the Z boson into neutrinos, constitutes an irreducible background. The first method to estimate this background from the data exploits the electroweak correspondence between the Z boson and the photon at high p_T, where they exhibit similar characteristics, apart from electroweak coupling differences and asymptotically vanishing residual mass effects [42]. The cross-section ratio between the Z-boson and photon production provides a robust prediction of the missing transverse momentum spectrum for invisible Z bosons at high p_T, where the photon production cross section is asymptotically about 20% less than the one for inclusive Z-boson production. One important distinction between photon and Z-boson production arises from the breakdown of the leading-order calculation of the γ+jets process for small-angle or vanishing-energy emission of the photon in the absence of a mass to regularize the resulting divergences. This can be mitigated by imposing isolation requirements on the selected photon sample.
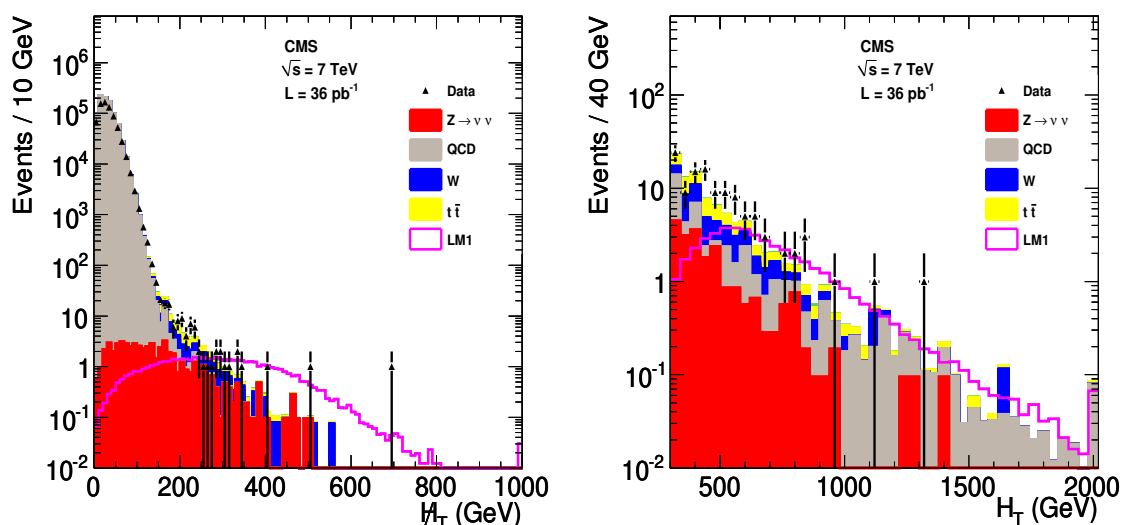
Figure 1. The (left) $\not{H}_T$ and (right) H_T distributions for the data and MC simulation samples with all baseline selection cuts applied except the $\not{H}_T$ and H_T requirements, respectively. The distributions for the individual backgrounds are shown separately, along with the predicted distributions for the LM1 SUSY point. However, these simulated distributions are not used to estimate the backgrounds in this analysis. Instead, the backgrounds are determined directly from the data.

The γ+jets control sample is collected using single-photon triggers, which were measured to be fully efficient for events passing the baseline selection. In the offline selection, photon candidates are distinguished from electrons by a veto on the presence of a track seed in the pixel detector. Photons from QCD multijet events are suppressed by requiring them to be isolated and the shower shape in the η coordinate to be consistent with that of a single photon [43].

For the derivation of the Z/γ cross-section correction factor, simulated γ+jets and $Z \to \nu\bar{\nu}$ MADGRAPH samples are used, in addition to the QCD multijet, W/Z+jets, and $t\bar{t}$ samples. The contribution of fragmentation photons, which do not have a counterpart in the massive Z-boson production, is estimated from NLO JETPHOX [44] calculations to be $(5 \pm 1)\%$ [45] in the selected photon sample. A second background arises from isolated neutral pions and η mesons decaying to pairs of secondary photons. For high-momentum mesons, these photon pairs are sufficiently well collimated to be reconstructed as a single photon. Using a method that fits a photon isolation observable to the expected distributions for real and background photons, the purity of the prompt photon sample is found to be $(94^{+6}_{-9})\%$ after the baseline selection, which is in good agreement with simulation. Finally, the background from electrons mis-identified as photons is measured with $Z \to e^+e^-$ data events and is found to be negligible for the search selections.

In order to predict the number of $Z(\nu\bar{\nu})$+jets events passing the search selections, the selected γ+jets control sample needs the following corrections after the background subtraction. First, the cross-section ratio between the $Z(\nu\bar{\nu})$+jets and γ+jets processes

		Baseline selection		High-$H\!\!\!/_{\mathrm{T}}$ selection		High-H_{T} selection	
Z/γ correction	±theory	0.41	±6 %	0.48	±6 %	0.44	±4 %
	±acceptance		±5 %		±5 %		±5 %
	±MC stat.		±7 %		±13 %		±13 %
Fragmentation		0.95	±1 %	0.95	±1 %	0.95	±1 %
Secondary photons		0.94	±9 %	0.97	±10 %	0.90	±9 %
Photon mistag		1.00	±1 %	1.00	±1 %	1.00	±1 %
Photon identification and isolation efficiency		1.01	±2 %	1.01	±2 %	1.01	±2 %
Total correction		0.37	±14 %	0.45	±18 %	0.38	±17 %

Table 2. Overview of all correction factors and corresponding systematic uncertainties for the prediction of the Z($\nu\bar{\nu}$) +jets background from the γ+jets control sample for each of the selections.

is estimated from simulation. The photon selection and isolation cuts are applied to the simulated samples when estimating this correction factor, hence folding the detector acceptance correction into this Z/γ correspondence. The correction factors for the baseline, the high-$H\!\!\!/_{\mathrm{T}}$, and the high-H_{T} selections are 0.41 ± 0.03, 0.48 ± 0.06, and 0.44 ± 0.06, respectively, where the uncertainties are statistical only. The uncertainty on the acceptance is taken as 5% [17], while the theoretical uncertainty is estimated from a comparison of leading to next-to-leading-order calculations of the ratio of Z and γ production with two jets [46]. This dedicated calculation was performed for the different selections in this analysis adapted to only two jets. The addition of an extra jet is mostly insensitive to the nature of the boson, and is not expected to induce a significant effect on the cross-section ratio. This leads to a 10% theoretical uncertainty on the Z/γ cross-section ratio for the baseline selection, which is taken as a uniformly distributed systematic uncertainty with a standard deviation of 6%. The photon reconstruction inefficiency is estimated in ref. [45] to be $(3.5 \pm 1.4)\%$. Finally, the photon identification and isolation efficiency is corrected for the difference between data and simulation. The correction is determined [43] to be 1.01 ± 0.02, after baseline selection.

In table 2 the full list of corrections is summarized for the baseline and search selections, along with the corresponding systematic uncertainties. The results for the Z($\nu\bar{\nu}$)+jets prediction from the γ+jets control sample are summarized in table 3. The prediction is in good agreement with the one found directly from the MC simulation, also given in table 3.

A potential alternative method to estimate the Z($\nu\bar{\nu}$)+jets background in a conceptually more straightforward way uses Z($\ell^+\ell^-$)+jets data events. By counting the pair of leptons as missing transverse momentum, the topology of the Z $\to \nu\bar{\nu}$ process can be reproduced, and all jet-related selection criteria can be directly applied. Only a small number of Z($\ell^+\ell^-$)+jets events pass the selection criteria in the currently available data. After the baseline selection, applying Z $\to \ell^+\ell^-$ selection requirements and correcting for the acceptance, efficiencies, and different branching fractions, the predicted Z $\to \nu\bar{\nu}$ rates are found to be compatible with the simulation predictions within uncertainties. However, none of the Z $\to$ e$^+$e$^-$ and Z $\to \mu^+\mu^-$ events pass either of the search selections.

	Baseline selection	High-H_T selection	High-H_T selection
γ+jets data sample	72	16	22
$Z \to \nu\bar{\nu}$ estimate from data	$26.3 \pm 3.2 \pm 3.6$	$7.1 \pm 1.8 \pm 1.3$	$8.4 \pm 1.8 \pm 1.4$
$Z \to \nu\bar{\nu}$ MC expectation	21.1 ± 1.4	6.3 ± 0.8	5.7 ± 0.7

Table 3. Number of γ+jets events in the data and the resulting estimate of the $Z(\nu\bar{\nu})$+jets background, as well as the prediction from the MC simulation, for each of the selections, with their statistical and systematic uncertainties. The estimate from data is obtained by multiplying the number of events in the γ+jets sample with the total correction factor from table 2.

More events can be used for predicting the $Z(\nu\bar{\nu})$+jets background by using $W(\ell\nu)$+jets events. This third method requires additional corrections for the W-Z correspondence and the $t\bar{t}$ contamination in the ℓ+jets control sample. With the available data, a few events are selected in the control samples for the search regions. The predicted number of $Z(\nu\bar{\nu})$+jets background events from this method is consistent with the predictions from the γ+jets events and the simulation.

5 W and $t\bar{t}$ background estimation

The muon and electron vetoes described in section 3.2 aim to suppress SM events with an isolated lepton. The W+jets and $t\bar{t}$ events, however, are not rejected by this lepton veto when a lepton from a W or top-quark decay is outside the geometric or kinematic acceptances, not reconstructed, not isolated (these three cases are denoted as a "lost lepton"), or is a tau lepton that decays hadronically (denoted as τ_h). In this section, two methods are presented to estimate these two components of the W+jets and $t\bar{t}$ backgrounds from data. The first method uses a μ+jets control sample, after correcting for lepton inefficiencies, to estimate the number of events that fail the isolated lepton reconstruction. The other method predicts the hadronic τ background from a similar μ+jets control sample by substituting a τ jet for the muon. For both methods the chosen μ+jets control sample fully represents the hadronic and other properties of the background it predicts.

The sum of the lost-lepton and hadronic-τ predictions yields an estimate for the sum of the W+jets and $t\bar{t}$ background. The $t\bar{t}$ contribution is also measured separately as a cross-check. The method predicts the $t\bar{t}$ background from a b-tagged control sample by correcting for the b-tag efficiency, acceptance, and the residual Z, W, and multijet contamination. Using the W-to-$t\bar{t}$ ratio predicted by simulation, the result is found to be consistent with the estimates described in the subsequent sections.

5.1 The W/$t\bar{t} \to e, \mu$+X background estimation

The muon control sample used to measure the W/$t\bar{t} \to e, \mu$+X background is selected by requiring exactly one muon that is isolated and passes the identification quality cuts discussed in section 3.2. From simulation, more than 97% of this sample are W+jets and $t\bar{t}$ events. In order to estimate the number of events in the signal region with non-isolated,

Isolation & identification efficiencies	-13%	$+14\%$
Kinematic differences between W, $t\bar{t}$, Z samples	-10%	$+10\%$
SM background in μ control sample	-3%	$+0\%$
MC use for acceptance calculation	-5%	$+5\%$
Total systematic uncertainty	-17%	$+18\%$

Table 4. Systematic uncertainties for the prediction of the lost-lepton background from the μ+jets control sample.

but identified electrons and muons, events in the isolated-muon control sample are weighted according to $\left(\frac{\epsilon_{\mathrm{ID}}^{\mathrm{e},\mu}}{\epsilon_{\mathrm{ID}}^{\mu}}\right)\left(\frac{1-\epsilon_{\mathrm{ISO}}^{\mathrm{e},\mu}}{\epsilon_{\mathrm{ISO}}^{\mu}}\right)$, where $\epsilon_{\mathrm{ISO}}^{\mathrm{e},\mu}$ are the electron and muon isolation efficiencies and $\epsilon_{\mathrm{ID}}^{\mathrm{e},\mu}$ the corresponding identification efficiencies. To model the number of events in the signal sample containing non-identified electrons or muons, the control sample is corrected by the factor $\left(\frac{1}{\epsilon_{\mathrm{ISO}}^{\mu}}\right)\left(\frac{1-\epsilon_{\mathrm{ID}}^{\mathrm{e},\mu}}{\epsilon_{\mathrm{ID}}^{\mu}}\right)$.

The lepton isolation efficiency is measured from $Z \rightarrow \ell^+\ell^-$ events using a tag-and-probe method [47] as a function of lepton p_{T} and the angular distance between the lepton and the nearest jet. The lepton identification efficiency is parametrized as a function of lepton p_{T} and η. Using these parametrizations, the efficiencies measured in Z events can be applied to the kinematically different W+jets and $t\bar{t}$ events.

Leptons can be out of the acceptance because either their transverse momentum is too small or they are emitted in the forward direction. Electrons and muons from τ decays in particular tend to have low momentum, while the additional neutrinos add to the $H\!\!\!/_{\mathrm{T}}$ of the event. The ratio R_{Accept} of events with out-of-acceptance leptons to those within the acceptance is estimated using simulation. The same muon control sample described above is used, weighted by R_{Accept} and corrected for the isolation and identification efficiencies, to estimate the background from out-of-acceptance leptons.

The dominant uncertainties on the lost-lepton prediction arise from the statistical uncertainties of both the control sample and the Z sample from which the lepton efficiencies are measured. Using simulation studies a systematic uncertainty is assigned to the kinematic differences that remain after the lepton-efficiency parametrization in the p_{T} and η spectra of the signal and control regions of the Z, W and $t\bar{t}$ samples. The residual presence of QCD, Z, or diboson events in the control sample is taken into account as a systematic uncertainty. Finally, the systematic uncertainty due to the use of the simulation in the acceptance correction is considered. All uncertainties are summarized in table 4. The total systematic uncertainty amounts to approximately 18%.

The prediction from this method applied to the muon control sample collected using the same H_{T} triggers as for the search is compared in table 5 to a prediction from simulated W+jets and $t\bar{t}$ events using the same method, and to the direct prediction from two different MC simulations. When applied to simulation, the method reproduces within the uncertainties the direct expectations from the simulation. Using the prediction from data after the baseline selection, about 50% more events are predicted than expected from the PYTHIA and MADGRAPH simulated samples. The difference is due to the generator parameter tune in the MC samples that were used to perform the comparison.

	Baseline selection	High-$H̸_T$ selection	High-H_T selection
Estimate from data	$33.0 \pm 5.5\,^{+6.0}_{-5.7}$	$4.8 \pm 1.8\,^{+0.8}_{-0.6}$	$10.9 \pm 3.0\,^{+1.7}_{-1.7}$
Estimate from MC (PYTHIA)	$22.9 \pm 1.3\,^{+2.7}_{-2.6}$	$3.2 \pm 0.4\,^{+0.5}_{-0.5}$	$7.2 \pm 0.7\,^{+1.1}_{-1.1}$
MC expectation (PYTHIA)	23.6 ± 1.0	3.6 ± 0.3	7.8 ± 0.5
Estimate from MC (MADGRAPH)	$22.9 \pm 1.4\,^{+2.9}_{-2.8}$	$2.7 \pm 0.4\,^{+0.4}_{-0.4}$	$5.4 \pm 0.5\,^{+0.7}_{-0.6}$
MC expectation (MADGRAPH)	23.7 ± 0.8	3.4 ± 0.3	6.5 ± 0.5

Table 5. Estimates of the number of lost-lepton background events from data and simulation for the baseline and search selections, with their statistical and systematic uncertainties.

5.2 The $W/t\bar{t} \to \tau_h + X$ background estimation

Hadronically decaying tau leptons constitute an important second component of the W and $t\bar{t}$ background. In this section a method is described to estimate the hadronic-τ background from a μ+jets control sample, mainly composed of $W(\mu\nu)$+jets and $t\bar{t}(\mu\nu)$+jets events. This muon control sample is selected from data collected with single-muon triggers, ensuring independence from the hadronic activity in the event. Events are required to have exactly one muon with $p_T > 20\,\text{GeV}$ and $|\eta| < 2.1$ and to satisfy the identification and isolation requirements described in section 3.2.

Jets from tau leptons are characterized by a low multiplicity of particles, typically a few pions and neutrinos. The hadronic properties of events in the hadronic-τ background are identical to those of the muon control sample, except for the fraction of the τ-jet energy deposited in the calorimeters. To account for this difference, each muon in the control sample is replaced by a τ-jet-like object. This object is built by scaling the muon momentum by a factor obtained from a simulated energy response distribution that models the fraction of visible momentum as a function of the true lepton momentum [48, 49]. The object is then added to the list of jets, and taken into account when applying the selection cuts to obtain the hadronic-τ background prediction from these modified events. In order to probe the full response distribution, this procedure is repeated multiple times for each event.

A correction is applied for the kinematic and geometric acceptances of the muons in the control sample. It is determined by applying a muon smearing procedure to events in W and $t\bar{t}$ simulated samples with a muon from W decay passing the muon kinematic selection, and comparing the resulting yield to the one obtained using all muons from W decay in the same events. The resulting correction factor is 0.84 ± 0.05 for the baseline and high-$H̸_T$ selection, and 0.89 ± 0.05 for the high-H_T selection. A second correction takes into account the muon trigger, reconstruction, and isolation efficiencies. The same procedure described in section 5.1 is followed. A correction is also applied for the relative branching fractions of W decays into muons or hadronic τ jets. For the simulated events a factor of 0.65 is used in the generation of the events and as the correction factor, while for data a factor of 0.69 is applied [50].

	Baseline selection	High-$H\!\!\!/_{\mathrm{T}}$ selection	High-H_{T} selection
τ response distribution	2%	2%	2%
Acceptance	+6%/−5%	+6%/−5%	+6%/−5%
Muon efficiency in data	1%	1%	1%
SM background subtraction	5%	5%	5%

Table 6. Systematic uncertainties for the hadronic-τ background prediction from the μ+jets control sample for the baseline and search selections.

	Baseline selection	High-$H\!\!\!/_{\mathrm{T}}$ selection	High-H_{T} selection
W/t$\bar{\mathrm{t}} \to \tau_{\mathrm{h}}$ estimate from data	$22.3 \pm 4.0 \pm 2.2$	$6.7 \pm 2.1 \pm 0.5$	$8.5 \pm 2.5 \pm 0.7$
W/t$\bar{\mathrm{t}} \to \tau_{\mathrm{h}}$ MC expectation	19.9 ± 0.9	3.0 ± 0.4	5.5 ± 0.5

Table 7. Predicted number of hadronic-τ background events from data and simulation for the baseline and search selections, with their statistical and systematic uncertainties.

The procedure for predicting the hadronic-τ background was tested on simulated W and t$\bar{\mathrm{t}}$ events and reproduces the direct results from the simulation of genuine hadronic tau leptons from W and t$\bar{\mathrm{t}}$ decays within uncertainties. For the baseline selection this uncertainty amounts to 12% and 3% for the W and t$\bar{\mathrm{t}}$ samples, respectively. The evaluation of the statistical uncertainty on the prediction needs special attention owing to the multiple sampling of the response distribution. This uncertainty is evaluated with a set of pseudo-experiments using the so-called bootstrap technique [51].

The systematic uncertainties and their impact on the prediction are summarized in table 6. The possible difference between data and simulation for the τ energy distribution is taken into account as a systematic uncertainty, estimated by scaling the visible energy fraction by 3% [52], resulting in a variation in the $H\!\!\!/_{\mathrm{T}}$ prediction of 2%. Possible SM background contamination in the muon control region comes from Z $\to \mu^+\mu^-$, t$\bar{\mathrm{t}}$/W+X $\to \tau\nu$+X $\to \mu\nu$+X, and from QCD multijet events. The first two are subtracted using the MC simulation, while the QCD multijet background is studied using an orthogonal control sample of events with non-isolated muons. The main source of background is W $\to \tau\nu \to \mu\nu$, estimated to be 10% of the total control sample. The number of W/t$\bar{\mathrm{t}} \to \tau_{\mathrm{h}}$+X events predicted in data using this method is summarized in table 7 for the different signal regions.

6 QCD background estimation

Two methods are employed to estimate the QCD multijet contamination in this analysis. The "rebalance-and-smear" (R&S) method estimates the multijet background directly from the data. This method predicts the full kinematics in multijet events, while being unaffected by events with true missing transverse momentum, including the potential presence of a

signal. Crucial inputs to this method are the jet energy resolutions, which are measured from data, including the non-Gaussian tails. The "factorization method" provides an alternative prediction for the QCD multijet background, based on the extrapolation from a lower-$H\!\!\!/_{\rm T}$ control region to the high-$H\!\!\!/_{\rm T}$ search region using the correlation between $H\!\!\!/_{\rm T}$ and an angular variable.

6.1 The rebalance-and-smear method

Large missing transverse momentum arises in QCD multijet events when one or more jets in the event have a jet energy response far from unity, where the jet energy response is the ratio of the transverse momentum of the reconstructed jet over the one which would result from measuring perfectly the four-momenta of the particles in the jet ("particle jet"). The R&S method is essentially a simplified simulation where the jet energy response is modelled by a parametrized resolution function, which is used to smear a sample of "seed events" obtained from data and consisting of "seed jets" that are good estimators of the true particle-jet momenta.

The seed events are produced in the "rebalance" step with an inclusive multijet data sample as input. This sample is selected from events collected using the triggers described in section 3.1, by requiring, in addition, two or more jets with $p_{\rm T} > 10\,{\rm GeV}$. Using the resolution probability distribution r, these seed events are constructed by adjusting the jet momenta in events with n jets given the likelihood $\mathcal{L} = \prod_{i=1}^{n} r(p_{{\rm T},i}^{\rm reco}|p_{{\rm T},i}^{\rm true})$, where $p_{{\rm T},i}^{\rm reco}$ and $p_{{\rm T},i}^{\rm true}$ are the reconstructed and true jet transverse momentum, respectively. The likelihood is maximized as a function of $p_{{\rm T},i}^{\rm true}$, subject to the transverse momentum balance constraint $\sum_{i=1}^{n} \vec{p}_{{\rm T},i}^{\rm true} + \vec{p}_{{\rm T,soft}}^{\rm true} = 0$. Here, all clustered objects with $p_{\rm T} > 10\,{\rm GeV}$ are classified as jets and $\vec{p}_{{\rm T,soft}}^{\rm true}$, which is the true transverse momentum of the rest of the event, can be approximated by the measured $\vec{p}_{{\rm T,soft}}^{\rm reco}$ that comprises all particles not included in the jets. In other words, the rebalancing step solves for the true momenta that bring the event into transverse momentum balance, in a way consistent with measurement uncertainties. This forces events with genuine high $H\!\!\!/_{\rm T}$ from neutrinos or other undetected particles to be similar to well-balanced QCD-like events. As such, $t\bar{t}$, W+jets, and Z+jets events, and also contributions from new physics, if any, have negligible impact on the background prediction since their production rate is much smaller than the QCD multijet production rate.

Most of the events in the seed sample consist of jets with responses well within the core of the resolution distribution. Because of this, the Gaussian resolution model for r is sufficient in the computation of the likelihood. A correction is needed, though, because jets near masked ECAL cells have an energy response below unity and hence get systematically rebalanced to too-low energies. To mitigate the resulting bias, each event is randomized in ϕ after rebalancing, such that well-rebalanced events dominate everywhere. A second correction to the rebalancing procedure is applied to account for the migration of reconstructed events towards higher $H_{\rm T}$ due to residual resolution smearing effects. This is achieved by inserting an additional term into the likelihood function, with parameters tuned to make the predicted jet multiplicity distribution match the one observed in the inclusive data sample. This correction induces less than a 5% change in the resulting distributions from data.
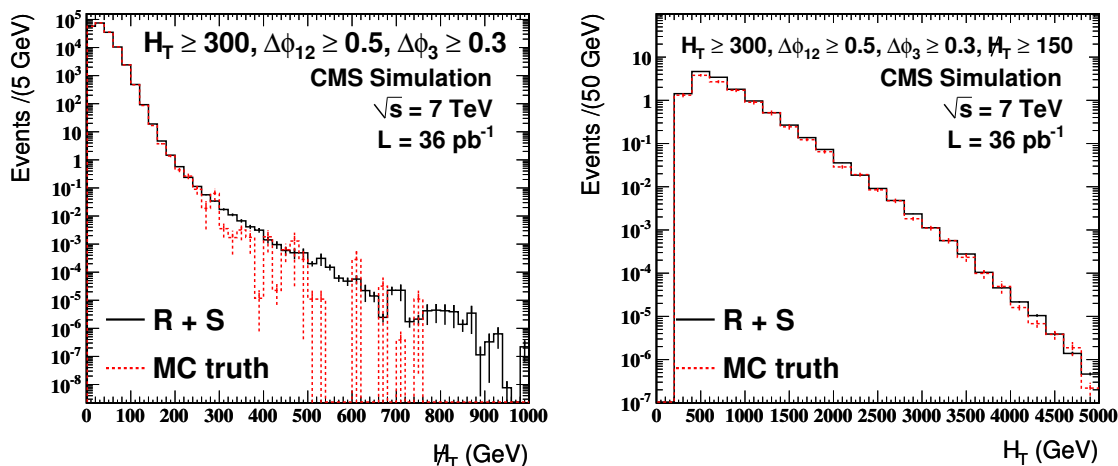
Figure 2. The (left) $\not{H}_T$ and (right) H_T distributions from the R&S method applied to simulation events, compared to the actual MC distribution (MC truth), for events passing ≥ 3 jets, $H_T \geq 300\,\text{GeV}$, and $\Delta\phi(\not{H}_T, \text{jet 1-3})$ selections, and additionally $\not{H}_T > 150\,\text{GeV}$ for the right plot.

Next, the momentum of each seed jet is smeared using the jet resolution distribution. The search requirements can be applied to the resulting smeared events to predict all event-by-event jet kinematic properties and correlations. This allows for flexibility in the set of observables used to define the search region, and in characterizing an observed signal. The distributions predicted by the R&S procedure are compared with those from MC simulation in figure 2. The predicted $\not{H}_T$ and H_T distributions are within 40% of the actual MC distributions in the search regions.

6.2 Jet response distributions

For smearing, and therefore the prediction of the $\not{H}_T$ spectrum, the full resolution functions including the non-Gaussian tails are used. The tails of the jet response function are of particular importance for the prediction of the QCD multijet background at high $\not{H}_T$.

The jet momentum resolution functions are parametrized using simulated PYTHIA di-jet samples and adjusted to match the measurements from data, as described below. The response distributions are parametrized with respect to p_T and η. Furthermore, an exceptionally low response arises at the specific $\eta - \phi$ locations where ECAL channels have been masked. This effect is taken into account by parametrizing the jet response as a function of the fraction $f_{\text{masked}}^{\text{ECAL}}$ of jet momentum lost in the masked area of the detector, computed using a template for the p_T-weighted distribution of particles as a function of the distance in η and ϕ to the jet axis. The dependence of the jet resolution on $f_{\text{masked}}^{\text{ECAL}}$ is shown in figure 3 (left). Finally, heavy-flavour b or c quarks and also gluons exhibit different jet resolution shapes than light jets, as shown in figure 3 (right). At high jet p_T, decays of heavy-flavour hadrons into neutrinos become one of the dominant sources of significant jet energy loss. The jet resolution functions are determined for bottom, charm, gluon, and other light-flavour quarks separately. The flavour dependence is then accounted for by us-
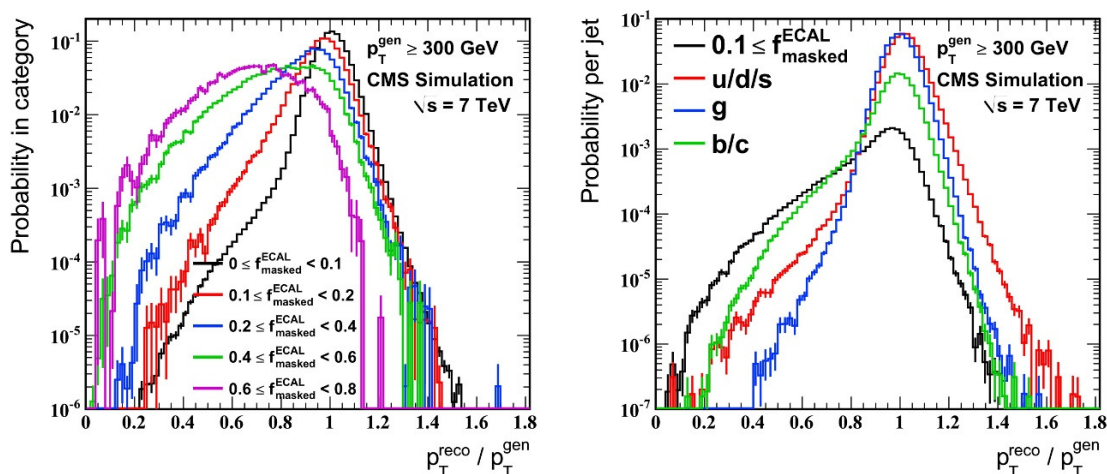
Figure 3. Ratio of the reconstructed jet transverse momentum to the generated transverse momentum for jets with $p_T^{gen} \geq 300\,\text{GeV}$. Distributions are shown for (left) different values of f_{masked}^{ECAL} and (right) gluons and different quark flavours.

ing these resolution functions in the smearing procedure according to the flavour fractions from simulation.

Two methods are used to measure from data a scaling factor for the Gaussian core of the jet momentum resolutions determined from simulation [31]. At low p_T, γ+jet events are used because the photons are reconstructed with excellent energy resolution and the p_T balance makes the photons good estimators of the true p_T scale of the event. At larger p_T, dijet events are used. An unbinned maximum likelihood fit is performed on the dijet asymmetry, $(p_T^{jet1} - p_T^{jet2})/(p_T^{jet1} + p_T^{jet2})$, with random ordering of the two highest-p_T jets. For both measurements the presence of additional jets in the event destroys the momentum balance and an extrapolation to no-additional-jet activity is performed. These methods measure the core of the Gaussian resolution as a function of jet η to be $5-10\%$ larger in data compared to simulation, with systematic uncertainties of similar size as the deviation. No significant dependence on the p_T of the jet is observed.

No significant non-Gaussian tails are observed in γ+jet events. At higher p_T, the dijet asymmetry distributions show compatibility within uncertainties between the resolution tails from data and simulation. Using the ratio of these asymmetry distributions in data and simulation, correction factors to the jet resolution tails from simulation are derived.

Both a scaling of the response below ("low" tail) and above unity ("high" tail) can induce the same change in the asymmetry distribution; the latter arising for instance from mismeasured track momenta in particle-flow jets. Therefore, the nominal resolution functions are obtained by equally scaling both the lower and upper tails of the resolution in order to induce the observed scaling of the asymmetry tail. The envelope of the variations induced by only low- or high-tail scaling is taken as the systematic uncertainty band for the jet resolution distribution.

	Baseline selection No $\Delta\phi$ cuts	Baseline selection	high-$H\!\!\!/_\mathrm{T}$ selection	high-H_T selection
N(PYTHIA)	138.6 ± 1.3	11.4 ± 0.4	0.13 ± 0.04	8.46 ± 0.32
N(R&S)	160.2 ± 0.1	13.2 ± 0.1	0.177 ± 0.004	9.57 ± 0.04
N(R&S)/N(PYTHIA)	1.16 ± 0.01	1.15 ± 0.04	1.4 ± 0.4	1.13 ± 0.05

Table 8. Number of events passing the various event selections from the PYTHIA multijet sample, the R&S method applied to the same simulated sample, and their ratio. The uncertainties quoted are statistical only.

6.3 Results of the rebalance-and-smear method

The performance of the R&S procedure was validated using simulated PYTHIA QCD multijet samples, without pileup interactions, where the parametrized response functions are derived from the same samples. The predicted and expected number of events are summarized for several selections in table 8. Before the $H\!\!\!/_\mathrm{T}$ requirement, the prediction of the H_T spectrum, the jet kinematics, and the jet-jet angular and p_T correlation distributions agree within 10% with the direct simulation. The $H\!\!\!/_\mathrm{T}$ distribution shows a bias up to 40%, which is mostly due to a dependency of the jet resolution on the presence of nearby jets. This is only of importance in the region of very high $H\!\!\!/_\mathrm{T}$, however, where the QCD multijet contribution is negligible compared to other backgrounds.

The QCD multijet background is predicted using the inclusive data sample with events passing the same H_T triggers described in section 3.1. The R&S steps are then executed using the jet energy resolution functions and the core and tail scale factors described in section 6.2. The background predictions are obtained by applying the event selection requirements to the R&S events. The rejection efficiency of events with large energy loss in masked ECAL channels is modelled using a parametrized per-jet probability from simulation.

In table 9 the number of predicted events is listed for the baseline and search regions, along with the relevant systematic uncertainties. Corrections are applied to the background estimates for several known biases in the method, as summarized in table 9. The largest one pertains to the smearing step, and arises from ambiguities in how the jet resolution is defined and from limitations in the parametrization. It is obtained in simulation by comparing the prediction from smeared particle jets with the corresponding one from the detector simulation. The size of the difference is taken as both a bias correction and a systematic uncertainty.

A second bias is intrinsic to the rebalancing procedure, and is studied by iterating the R&S method. A first iteration (R&S)[1] of the method gives a sample of pure QCD multijet events with known true jet resolution, i.e., by construction the one used in the smearing step. Performing a second iteration (R&S)[2] of the method on this (R&S)[1] sample, using the same resolutions, provides a closure test of just the rebalancing part when compared to the input (R&S)[1] events. The degree of non-closure, i.e. the excess of (R&S)[2] over (R&S)[1] predicted events, is measured to be 10%, which is also assigned as a systematic uncertainty.

		Baseline selection	high-$\slashed{H}_T$ selection	high-H_T selection
Nominal prediction (events)		39.4	0.18	19.0
Particle jet smearing closure	(box)	+14%	+30%	+7%
Rebalancing bias	(box)	+10%	+10%	+10%
Soft component estimator	(box)	+3%	+19%	+4%
Resolution core	(asymmetric)	+14% −25%	+0% −52%	+15% −21%
Resolution tail	(asymmetric)	+43% −33%	+56% −78%	+48% −34%
Flavour trend	(symmetric)	±1%	±12%	±0.3%
Pileup effects	(box)	±2%	±10%	±2%
Control sample trigger	(box)	−5%	−5%	−5%
Search trigger	(symmetric)	±1%	±1%	0%
Lepton veto	(box)	±5%	±0.05%	±0.2%
Seed sample statistics	(symmetric)	±2.3%	±23%	±3.3%
Total uncertainty		51%	64%	49%
Bias-corrected prediction (events)		29.7 ± 15.2	0.16 ± 0.10	16.0 ± 7.9

Table 9. Number of QCD multijet events predicted with the R&S method, before and after bias corrections, along with all considered uncertainties and the type of uncertainty (uniform "box"-like, symmetric or asymmetric Gaussian distribution). Effects in italics are the biases corrected for as described in the text, with the full size of the bias taken as the systematic uncertainty.

The same $(\text{R\&S})^2/(\text{R\&S})^1$ procedure is employed to study the bias caused by using $\vec{p}_{\mathrm{T,soft}}^{\mathrm{reco}}$ as an estimator of $\vec{p}_{\mathrm{T,soft}}^{\mathrm{true}}$. The true value of $\vec{p}_{\mathrm{T,soft}}^{\mathrm{true}}$ in the second iteration is equal to the $\slashed{H}_T$ value calculated from the rebalanced jets in the first iteration. The difference between the $(\text{R\&S})^2$ predictions with $\vec{p}_{\mathrm{T,soft}}^{\mathrm{reco}}$ and $\vec{p}_{\mathrm{T,soft}}^{\mathrm{true}}$ as input is used as a third bias correction, with corresponding systematic uncertainty.

The largest systematic effect arises from uncertainties on the jet momentum resolution. The measurement uncertainties on the core resolutions and non-Gaussian tails, discussed in section 6.2, are propagated by repeating the R&S prediction with resolution inputs varied within these uncertainties. Another systematic uncertainty comes from the flavour-dependent parametrization of the jet resolutions. It is evaluated as the difference between the use of PYTHIA and MADGRAPH simulated samples to derive the b- and c-quark content parametrization. These MC generators have heavy-flavour fractions that differ by roughly 25% for bottom and 50% for charm quarks. Nevertheless, the difference in the resulting background prediction is very small in the high-H_T search regions, and the QCD multijet contribution is negligible in the high-$\slashed{H}_T$ search region.

The effect of pileup is studied by performing the R&S prediction with a subset of events with exactly one reconstructed primary vertex. The relative difference between this prediction and the one obtained from the inclusive sample is taken as a systematic uncertainty.

Other smaller uncertainties arise from the event selection. A potential loss of events due to the H_T trigger requirement on the events that enter the rebalancing is quantified by comparing the prediction made with the small number of events collected with a low-p_T single-jet trigger. A conservative upper bound of 5% on this uncertainty is taken. Another uncertainty arises from the need to predict the number of smeared events that pass the search trigger. The H_T triggers used were measured on data to be fully efficient with respect to events passing the offline cuts, and the statistical upper bound from this measurement is taken as a systematic uncertainty for the low-H_T selections. Finally, the lepton veto has an uncertainty that is estimated as the full size of the rejection rate for QCD multijet events in a PYTHIA event sample with pileup conditions representative of the data. The large size of this uncertainty for the baseline search region is due to a near-100% statistical uncertainty induced by a MC sample with a very small equivalent luminosity.

Variations within one standard deviation or within upper and lower bounds are performed for each systematic effect, and the corresponding differences in the predictions are quoted in table 9. Estimated shapes of the probability distribution of each uncertainty are also listed; uncertainties that are estimated as upper bounds on possible effects are assumed to have a uniform "box"-like distribution. The statistical uncertainty is associated with the size of the seed event sample. As prescribed by the bootstrap method [51], an ensemble of pseudo-datasets is selected randomly from the original seed sample, allowing repetition. The ensemble spread of predictions made from these pseudo-datasets is taken as the statistical uncertainty.

After correcting for biases, the R&S prediction and systematic uncertainties are combined via a numerical integration MC technique, which takes properly into account non-Gaussian distributed uncertainties. The mean and r.m.s. deviation of the resulting distributions of the expected number of multijet background events for the baseline and search selections are taken as the central values and uncertainties of the final R&S prediction, as given in the last row of table 9. These central values are slightly shifted compared to the nominal bias-corrected values owing to the asymmetrically distributed uncertainties.

6.4 The factorization method

Because of the importance of estimating the QCD multijet background, an independent approach is used as a cross-check. The factorization method uses the observables $\not{H}_T$ and $\Delta\phi_{\min}$, of which the latter is the minimum azimuthal angle between the $\not{H}_T$ direction and the three leading jets, to predict the number of events in the signal region of high $\not{H}_T$ and large $\Delta\phi_{\min}$ from the sideband regions where one or both variables are small. As $\not{H}_T$ and $\Delta\phi_{\min}$ are not independent observables, their correlation is measured in the low-$\not{H}_T$ region by means of the ratio $r(\not{H}_T)$ of the number of events with large $\Delta\phi_{\min}$ to the number with small $\Delta\phi_{\min}$. The number of background events is estimated from the extrapolation of r to the high-$\not{H}_T$ signal region.

The parametrization of $r(\not{H}_T)$ is chosen empirically, with two different ones being used. The first parametrization, the Gaussian model, predicts a Gaussian distribution for $\Delta\phi_{\min}$, assuming all jets, except the most mismeasured jet, to have an energy response following a Gaussian resolution function. The width of this distribution as a function of $\not{H}_T$ is described

Method	Baseline selection	High-$H\!\!\!/_T$ selection	High-H_T selection
Gaussian model	$19.0 \pm 1.6\,^{+7.2}_{-6.5}$	$0.3 \pm 0.1\,^{+0.4}_{-0.2}$	$13.0 \pm 1.3\,^{+4.9}_{-4.4}$
Exponential model	$31.4 \pm 2.4\,^{+7.0}_{-6.9}$	$0.5 \pm 0.1\,^{+0.2}_{-0.2}$	$21.6 \pm 2.0\,^{+4.8}_{-4.8}$
Combined	$25.2 \pm 2.4\,^{+13.2}_{-13.1}$	$0.4 \pm 0.1\,^{+0.3}_{-0.3}$	$17.3 \pm 2.0\,^{+9.1}_{-9.2}$

Table 10. Predictions for the number of QCD multijet background events using the factorization method with two different parametrizations and their combination, for the baseline and search selections, with their statistical and systematic uncertainties.

both in simulation and data by a falling exponential function, from which the functional form for $r(H\!\!\!/_T)$ is derived. An additional constant term, determined from a MadGraph QCD multijet simulation, is added to $r(H\!\!\!/_T)$ to keep it more-nearly constant at high values of $H\!\!\!/_T$. A large value of H_T is further required to suppress events with low-p_T jets at low $H\!\!\!/_T$. This method results in a prediction for a lower limit on the number of expected QCD multijet background events in the signal region, since any non-Gaussian tails in the $\Delta\phi_{\min}$ resolutions result in a larger estimate.

As an alternative to the Gaussian resolution model, $r(H\!\!\!/_T)$ is parametrized as an exponential plus the same constant term used in the Gaussian model. The same H_T cut is applied. The extrapolation to high $H\!\!\!/_T$ leads to a larger $r(H\!\!\!/_T)$ value than observed in the simulation. Various systematic variations of simulated QCD samples show that the true yield of the QCD multijet background is between the predictions from the two parametrizations.

The dominant uncertainty on the prediction is the statistical uncertainty from the data in the control region and the statistical uncertainties on the fit parameters. A systematic uncertainty arises from the constant term at high $H\!\!\!/_T$ for both models, which is estimated to be $+11\%/-6\%$ from a variety of different simulated samples. Further systematic uncertainties come from the SM background contamination in the control regions, $+4\%/-8\%$, and from the H_T requirement discussed above, $+0\%/-11\%$.

The predictions for the QCD multijet background from the two parametrizations are given in table 10 for the three different selections. The final background estimate is taken as the average of the two model predictions, with half the difference assigned as an additional systematic uncertainty and added linearly to the uncertainty on the combination. The results are in agreement with the predictions using the R&S method.

7 Results and interpretation

7.1 Results and limits

The number of events observed in data and the event yields predicted by the different background estimation methods are summarized in table 11 for the three different selections. The total background is calculated summing the QCD R&S, the $Z(\nu\bar{\nu})$+jets from photons,

Background process	Baseline selection	High-$H\!\!\!/_T$ selection	High-H_T selection
$Z(\nu\bar{\nu})$+jets (γ+jets method)	26.3 ± 4.8	7.1 ± 2.2	8.4 ± 2.3
$W/t\bar{t} \rightarrow e, \mu$+X	33.0 ± 8.1	4.8 ± 1.9	10.9 ± 3.4
$W/t\bar{t} \rightarrow \tau_h$+X	22.3 ± 4.6	6.7 ± 2.1	8.5 ± 2.5
QCD multijet (R&S method)	29.7 ± 15.2	0.16 ± 0.10	16.0 ± 7.9
Total background	111.3 ± 18.5	18.8 ± 3.5	43.8 ± 9.2
Observed in data	111	15	40
95% CL upper limit on signal	40.4	9.6	19.6

Table 11. Predicted number of background events from the different estimates for the baseline and search selections, their total, and the corresponding number of events observed in data. The background combination is performed as explained in the text. The uncertainties shown include both statistical and systematic uncertainties. The last line gives the 95% confidence level (CL) upper limit on the number of possible signal events.

and the $W/t\bar{t}$ lost-lepton and hadronic-τ estimates. No excess of events is observed in either the high-$H\!\!\!/_T$ or high-H_T search regions.

In order to derive limits on new physics, the expected number of signal events for the event selections are estimated using simulated signal samples, taking into account uncertainties on the event selection, theoretical uncertainties related to the event generation, and an overall luminosity uncertainty. Many of these uncertainties have a dependence on the event kinematics, and hence are model dependent.

The largest experimental contribution to the uncertainty on the signal expectation arises from the model-dependent jet energy scale and resolution uncertainties. These amount to 8% for the LM1 benchmark point. Smaller uncertainties are due to the lepton veto and the trigger. For the former a 2% uncertainty is determined for LM1; for the latter a conservative uncertainty of 1% is assigned. The inefficiency of the rejection of events with energy in masked ECAL cells is determined to be about 1.5% for the LM1 benchmark point. This full inefficiency is taken as the uncertainty, even though the ECAL masked-channel simulation reproduces well the effect in data [33]. For other event cleaning procedures, possible inefficiencies are determined in a low-$H\!\!\!/_T$ data control region to be negligible. Also the possible effect from the presence of additional pileup interactions corresponding to the LHC 2010 data-taking conditions was investigated and found to be insignificant. On the theoretical side, all uncertainties considered are model-dependent. The largest one is associated with the factorization and renormalization scale uncertainties on the next-to-leading-order cross-section corrections, yielding a 16% uncertainty for the LM1 point. Smaller contributions come from uncertainties on the parton distribution functions and initial-state radiation, respectively 3% and 2% for LM1. Final-state radiation uncertainties are found to be negligible. Finally, a luminosity uncertainty of 4% is accounted for [53], along with the statistical uncertainty on the simulated signal samples, which is about 2% for the LM1 sample.
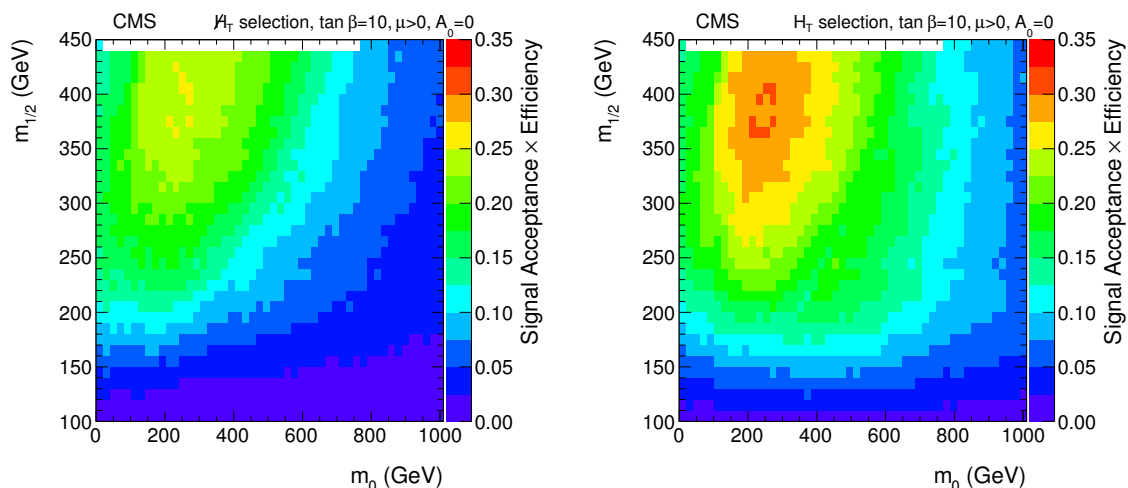
Figure 4. Total signal efficiency for the $\displaystyle{\not}H_T$ (left) and H_T (right) selections, as a function of m_0 and $m_{1/2}$. The other CMSSM parameters are $\tan\beta = 10$, $\mu > 0$, and $A_0 = 0$.

The probability distributions corresponding to each uncertainty source, whether Gaussian, bifurcated Gaussian, Poisson, or box shaped, are convolved using a numerical integration MC technique to obtain the probability distributions for each background and for the overall background estimation. The presence of several sources of uncertainties makes the overall combination quite Gaussian in shape, as expected from the central limit theorem. The resulting distribution is fitted to a Gaussian function, and the mean and standard deviation are used as the central value and uncertainty in the limit calculations described in the following sections. This last step is applied in order to obtain the best symmetric approximation to a distribution with a residual asymmetry.

7.2 Interpretation within the CMSSM

The parameters m_0 and $m_{1/2}$ of the CMSSM are varied in $10\,\mathrm{GeV}$ steps for three different values of $\tan\beta = 3$, 10, and 50. Leading-order IsaJet [54] signal cross sections are used and corrected by next-to-leading-order K factors calculated using Prospino [41]. The total signal efficiency, including geometrical acceptance and selection efficiency, varies over the CMSSM phase space, being in the range $20-30\%$ for the high-H_T selection and $10-20\%$ for the high-$\displaystyle{\not}H_T$ selection, as shown in figure 4.

The expected upper limits on the CMSSM cross section are calculated using the background estimate from data under the no-signal hypothesis. For the determination of the observed upper limit the signal contamination in the background estimate is corrected for. In the isolated-muon control region of the lost-lepton and hadronic-τ methods, the signal contamination is calculated and removed from the background estimate for each CMSSM parameter point. For both selections, the signal contributions to the background estimate are $2-3$ events for the lost leptons and $1-2$ events for the hadronic tau decays. The signal contamination in the γ+jets control region is found to be negligible. The QCD multijet background estimation with the R&S method is not affected by signal contamination.
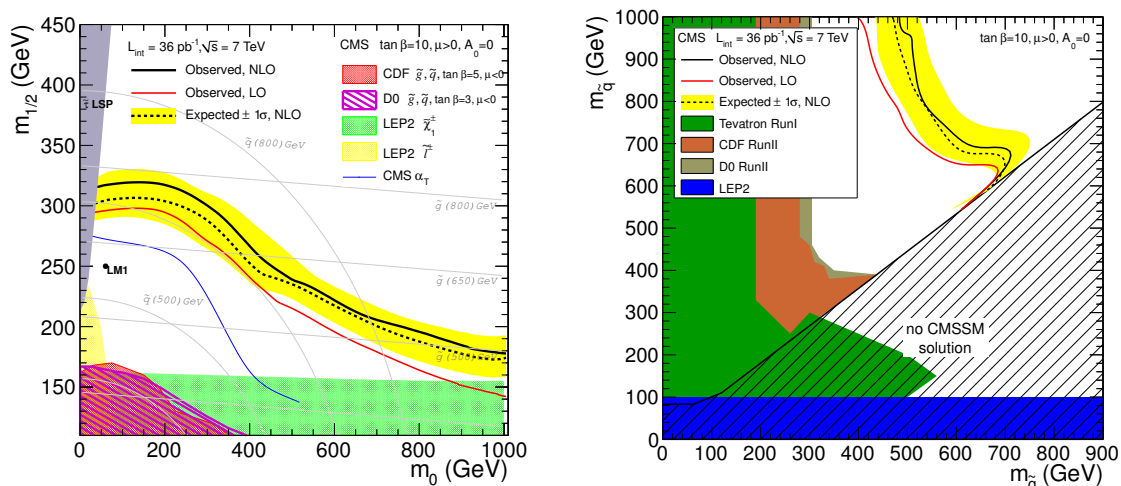
Figure 5. The expected and observed 95% CL upper limits in the CMSSM m_0–$m_{1/2}$ (left) and gluino-squark (right) mass planes for LO and NLO cross sections. The ± 1 standard deviation (σ) band corresponds to the expected limit. The contours are the combination of the H_T and the $\slashed{H}_T$ selections such that the contours are the envelope with respect to the best sensitivity. The CMSSM parameters are $\tan\beta = 10$, $\mu > 0$, and $A_0 = 0$. The limit from the earlier CMS analysis is shown as a blue line and limits from other experiments as the shaded regions. For the area labeled "$\tilde{\tau}$ LSP" the stau becomes the LSP. The LM1 SUSY benchmark scenario is shown as a point.

The modified frequentist procedure CLs [55, 56] with a likelihood ratio test-statistic is used for the limit calculation. In figure 5 the observed and expected CLs 95% confidence level (CL) upper limits are shown in the CMSSM m_0-$m_{1/2}$ (left) and the gluino-squark (right) mass planes for $\tan\beta = 10$, $\mu > 0$, and $A_0 = 0$. Limit contours for $\tan\beta = 3$ and $\tan\beta = 50$ can be found in [57]. The contours are the envelope with respect to the best sensitivity of both the H_T and the $\slashed{H}_T$ search selections. For $m_0 \lesssim 450\,\text{GeV}$ the $\slashed{H}_T$ selection is more powerful, while for large m_0 the H_T selection is more important. A 95% CL upper limit on the production cross section in the range between 2 and 3 pb is obtained, depending on the squark and gluino masses considered. Gluino masses below 500 GeV are excluded at 95% CL for squark masses below 1 000 GeV. A previously published search by CMS for supersymmetry in hadronic events [17] using the event shape observable α_T [16] is shown for reference. The α_T analysis aims at the best possible removal of the QCD multijet background, and is particularly powerful for small jet multiplicities and high missing transverse energy. Because of the high signal selection efficiency in a large fraction of the phase space, and in spite of the larger background compared to the α_T selection, the analysis presented here is able to improve the limits previously set by the α_T analysis.

7.3 Interpretation with Simplified Model Spectra

Models for new physics can also be studied in a more generic manner using a simplified model spectra (SMS) approach [23–26]. Simplified models are designed to characterize
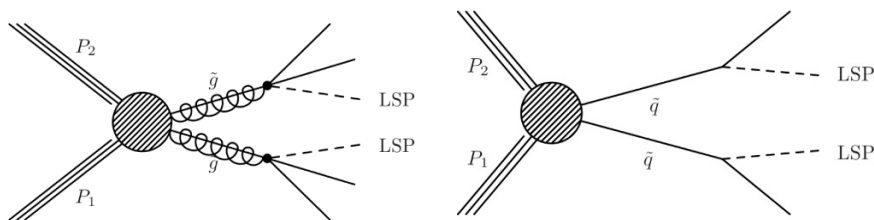
Figure 6. Diagrams of the studied simplified models. Left: gluino pair production; right: squark pair production.

experimental data in terms of a small number of basic parameters. They exploit the fact that at the LHC the final-state kinematics of events involving strongly produced massive new particles are largely determined by the parton distribution functions and phase-space factors associated with two- and three-body decays. Using these simplified models, the experimental results can then be translated into any desired framework.

For the simplified models used in this paper, it is assumed that the new particles are strongly produced in pairs whose decay chains ultimately result in a stable weakly interacting massive particle, denoted as LSP. The particles produced in the hard interaction can be identified as partners of quarks and gluons. In SUSY these would be the squarks ($\tilde{q}$) and gluinos ($\tilde{g}$). Even though the SMS are more generic, in the following everything is phrased for simplicity in terms of super-partner names. Two benchmark simplified models are investigated for the number of jets and $\not{H}_\mathrm{T}$ signature in this analysis: pair-produced gluinos, where each gluino directly decays to two light quarks and the LSP, and pair-produced squarks, where each squark decays to one light quark and the LSP. In figure 6 the respective diagrams for these simplified models are drawn. To limit the set of SMS studied, only a few are chosen that can bracket the kinematic properties of the different final states. For this reason the gluino-squark associated production is neglected.

The simplified models are simulated with the PYTHIA generator [35], the CTEQ6L1 parton distribution functions [58], and the parametrized CMS detector simulation. For each topology, samples are generated for a range of masses of the particles involved, and thus more mass splittings are explored than in the CMSSM, where the ratio of the gluino and the LSP masses is approximately fixed.

In the following, the measured cross section upper limits are compared to a typical reference next-to-leading-order cross section from PROSPINO [41]. In the case of squark pair production this reference cross section corresponds to the squark-antisquark cross section with four light flavours included, with the gluinos becoming nearly decoupled at 3 TeV. This cross section is used to convert upper limits on the production cross section to reference limits on new-particle masses.

In figure 7 the total signal efficiency of the high-$\not{H}_\mathrm{T}$ selection, including geometrical acceptance and selection efficiency, is shown within the simplified model space for gluino and squark pair production, as a function of the gluino (left) or squark mass (right) and
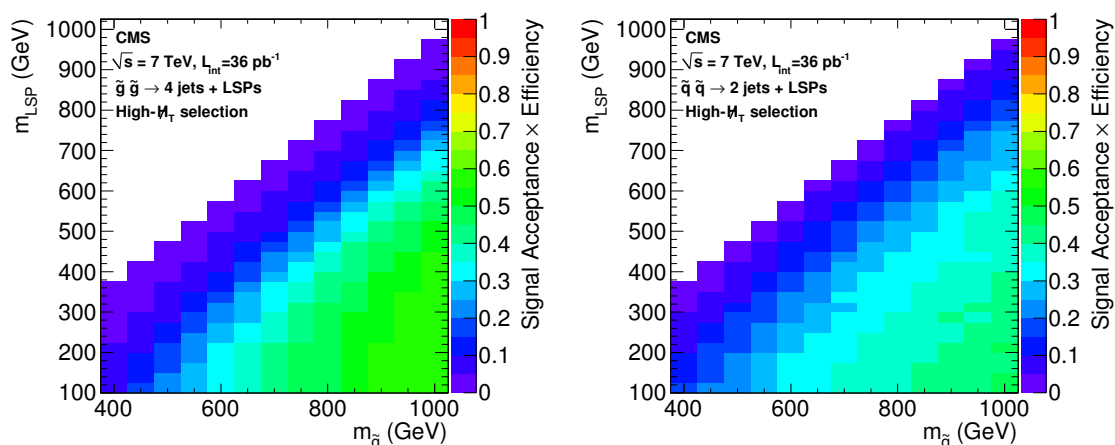
Figure 7. Total high-$\not{H}_T$ selection efficiency for gluino (left) and squark (right) production as a function of the gluino (left) or squark (right) mass and the LSP mass.

the LSP mass. Only the lower half of the plane is filled because the model is only valid when the gluino or squark masses are larger than the mass of the LSP. The signal selection efficiency increases for higher gluino and squark masses, and is low on the diagonal, where the mass splitting is small and jets are produced with lower transverse momentum.

The limit calculation in the SMS space is performed using a Bayesian framework with a flat prior for the signal [50]. The same sources of uncertainties affecting the signal geometrical acceptance and selection efficiency are incorporated for each scan point as for the CMSSM interpretation, namely the jet energy scale and resolution, the lepton veto, the cleaning including the veto on large energy loss in masked ECAL cells, the trigger, the initial- and final-state radiation, the parton distribution functions, the luminosity, and the statistical uncertainty. The estimation of the theoretical uncertainties is further detailed in [57]. The renormalization and factorization scale uncertainties do not apply here because they only influence the normalization of the reference cross section. The presence of signal events in the background sample is not considered, since the studied SMS processes do not produce prompt leptons or photons, and since the R&S method is insensitive to such contamination.

In figure 8 the exclusion 95% CL upper limits on the production cross sections are presented for the high-$\not{H}_T$ search selection. This selection is found to be more sensitive than the high-H_T search selection for both considered simplified model spectra. Cross sections in the range between 0.5 and 30 pb are excluded at 95% CL, depending on the masses of the new particles in the decay chains. In ref. [57] all the efficiencies, the combined experimental and theoretical uncertainties, and all limits can be found for both the high-$\not{H}_T$ and high-H_T event selections, and for both the gluino and squark pair-production simplified models. Using this model-independent representation with the simplified model spectra, these upper limits on the cross section can be translated into a limit on any complete model such as SUSY.
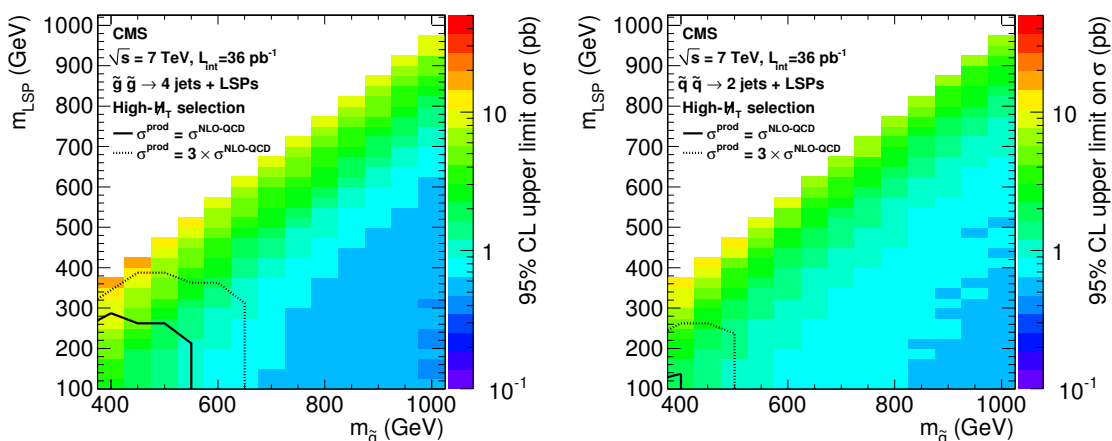
Figure 8. 95% CL upper limits on the gluino (left) and squark (right) pair-production cross sections for the high-$\not{H}_T$ selection, as a function of the gluino (left) or squark (right) mass and the LSP mass. The contours where the reference cross section and three times this cross section can be excluded are shown.

8 Conclusions

An inclusive search for new physics has been presented using events with a multijet signature with large missing transverse momentum. The observed event yield is consistent with the SM background contributions, arising mainly from $Z(\nu\bar{\nu})$+jets, $W(\ell\nu)$+jets, $t\bar{t}$ including a W that decays leptonically, and QCD multijet production. These SM contributions were estimated directly from the data using several novel techniques, giving a minimal reliance on simulation. The overall uncertainty on the resulting total background prediction is dominated by the statistical uncertainty.

In the absence of an excess of events above the expectation, upper limits are derived in the CMSSM parameter space. In R-parity conserving CMSSM with $A_0 = 0$, $\mu > 0$, and $\tan\beta = 10$, a 95% CL upper limit on the production cross section in the range between 2 and 3 pb is obtained, depending on the squark and gluino masses considered. Gluino masses below 500 GeV are excluded at 95% CL for squark masses below 1 000 GeV. Similar results are obtained for other $\tan\beta$ values. The results are also more generically interpreted in the context of simplified models where final states are described by the pair production of new particles which decay either to one or two jets and a dark-matter candidate escaping detection. We obtain a 95% CL upper limit on the production cross section for such new particles in the range between 0.5 and 30 pb, depending on the masses of the new particles in the decay chains.

Acknowledgments

We thank the members of the BLACKHAT collaboration for their input and fruitful discussions concerning vector boson production with jets at the LHC.

References

[1] J. Wess and B. Zumino, *Supergauge transformations in four-dimensions*, *Nucl. Phys.* **B 70** (1974) 39 [SPIRES].

[2] H.-C. Cheng and I. Low, *TeV symmetry and the little hierarchy problem*, *JHEP* **09** (2003) 051 [hep-ph/0308199] [SPIRES].

[3] T. Appelquist, H.-C. Cheng and B.A. Dobrescu, *Bounds on universal extra dimensions*, *Phys. Rev.* **D 64** (2001) 035002 [hep-ph/0012100] [SPIRES].

[4] J.L. Feng, *Dark matter candidates from particle physics and methods of detection*, *Ann. Rev. Astron. Astrophys.* **48** (2010) 495 [arXiv:1003.0904] [SPIRES].

[5] CDF collaboration, T. Aaltonen et al., *Inclusive search for squark and gluino production in $p\bar{p}$ collisions at $\sqrt{s} = 1.96\,TeV$*, *Phys. Rev. Lett.* **102** (2009) 121801 [arXiv:0811.2512] [SPIRES].

[6] D0 collaboration, V.M. Abazov et al., *Search for squarks and gluinos in events with jets and missing transverse energy using $2.1\,fb^{-1}$ of $p\bar{p}$ collision data at $\sqrt{s} = 1.96\,TeV$*, *Phys. Lett.* **B 660** (2008) 449 [arXiv:0712.3805] [SPIRES].

[7] D0 collaboration, V.M. Abazov et al., *Search for associated production of charginos and neutralinos in the trilepton final state using $2.3\,fb^{-1}$ of data*, *Phys. Lett.* **B 680** (2009) 34 [arXiv:0901.0646] [SPIRES].

[8] UA1 collaboration, C. Albajar et al., *Events with large missing transverse energy at the CERN collider. 3. Mass limits on supersymmetric particles*, *Phys. Lett.* **B 198** (1987) 261 [SPIRES].

[9] UA2 collaboration, R. Ansari et al., *Search for exotic processes at the CERN $p\bar{p}$ collider*, *Phys. Lett.* **B 195** (1987) 613 [SPIRES].

[10] ALEPH collaboration, A. Heister et al., *Absolute mass lower limit for the lightest neutralino of the MSSM from e^+e^- data at $\sqrt{s}$ up to 209 GeV*, *Phys. Lett.* **B 583** (2004) 247 [SPIRES].

[11] DELPHI collaboration, J. Abdallah et al., *Searches for supersymmetric particles in e^+e^- collisions up to 208 GeV and interpretation of the results within the MSSM*, *Eur. Phys. J.* **C 31** (2003) 421 [hep-ex/0311019] [SPIRES].

[12] L3 collaboration, P. Achard et al., *Search for scalar leptons and scalar quarks at LEP*, *Phys. Lett.* **B 580** (2004) 37 [hep-ex/0310007] [SPIRES].

[13] OPAL collaboration, G. Abbiendi et al., *Search for chargino and neutralino production at $\sqrt{s} = 192\,GeV$ to 209 GeV at LEP*, *Eur. Phys. J.* **C 35** (2004) 1 [hep-ex/0401026] [SPIRES].

[14] ZEUS collaboration, S. Chekanov et al., *Search for stop production in R-parity-violating supersymmetry at HERA*, *Eur. Phys. J.* **C 50** (2007) 269 [hep-ex/0611018] [SPIRES].

[15] H1 collaboration, S. Aid et al., *A search for selectrons and squarks at HERA*, *Phys. Lett.* **B 380** (1996) 461 [hep-ex/9605002] [SPIRES].

[16] L. Randall and D. Tucker-Smith, *Dijet searches for supersymmetry at the LHC*, *Phys. Rev. Lett.* **101** (2008) 221803 [arXiv:0806.1049] [SPIRES].

[17] CMS collaboration, V. Khachatryan et al., *Search for supersymmetry in pp collisions at $7\,TeV$ in events with jets and missing transverse energy*, *Phys. Lett.* **B 698** (2011) 196 [arXiv:1101.1628] [SPIRES].

[18] ATLAS collaboration, *Search for squarks and gluinos using final states with jets and missing transverse momentum with the ATLAS detector in $\sqrt{s} = 7$ TeV proton-proton collisions*, accepted by *Phys. Lett.* **B** (2011).

[19] A.H. Chamseddine, R.L. Arnowitt and P. Nath, *Locally supersymmetric grand unification*, *Phys. Rev. Lett.* **49** (1982) 970 [SPIRES].

[20] R.L. Arnowitt and P. Nath, *SUSY mass spectrum in* SU(5) *supergravity grand unification*, *Phys. Rev. Lett.* **69** (1992) 725 [SPIRES].

[21] G.L. Kane, C.F. Kolda, L. Roszkowski and J.D. Wells, *Study of constrained minimal supersymmetry*, *Phys. Rev.* **D 49** (1994) 6173 [hep-ph/9312272] [SPIRES].

[22] G.L. Kane, C.F. Kolda, L. Roszkowski and J.D. Wells, *Dark matter from supersymmetric grand unification*, hep-ph/9405363 [SPIRES].

[23] J. Alwall, P. Schuster and N. Toro, *Simplified models for a first characterization of new physics at the LHC*, *Phys. Rev.* **D 79** (2009) 075020 [arXiv:0810.3921] [SPIRES].

[24] J. Alwall, M.P. Le, M. Lisanti and J.G. Wacker, *Searching for gluinos at the Tevatron and beyond*, *Int. J. Mod. Phys.* **A 23** (2008) 4637 [SPIRES].

[25] D. Alves et al., *Simplified Models for LHC New Physics Searches*, arXiv:1105.2838 [SPIRES].

[26] N. Arkani-Hamed et al., *MARMOSET: The path from LHC data to the new standard model via on-shell effective theories*, hep-ph/0703088 [SPIRES].

[27] CMS collaboration, *The CMS experiment at the CERN LHC*, *JINST* **08** (2008) S08004.

[28] CMS collaboration, *Particle-flow event reconstruction in CMS and performance for jets, taus, and E_{T}^{miss}*, *CMS Physics Analysis Summary* **CMS-PAS-PFT-09-001** (2009).

[29] M. Cacciari, G.P. Salam and G. Soyez, *The anti-k_t jet clustering algorithm*, *JHEP* **04** (2008) 063 [arXiv:0802.1189] [SPIRES].

[30] M. Cacciari, *FastJet: a code for fast k_t clustering and more*, hep-ph/0607071 [SPIRES].

[31] CMS collaboration, S. Chatrchyan et al., *Determination of jet energy calibration and transverse momentum resolution in CMS*, submitted to *JINST* (2011) [arXiv:1107.4277] [SPIRES].

[32] CMS collaboration, *Electromagnetic calorimeter commissioning and first results with 7 TeV data*, *CMS Note* **2010-012** (2010).

[33] CMS collaboration, S. Chatrchyan et al., *Missing transverse energy performance of the CMS detector*, submitted to *JINST* (2011) [arXiv:1106.5048] [SPIRES].

[34] S. Agostinelli et al., *G4 — a simulation toolkit*, *Nucl. Instrum. and Meth.* **506** (2003) 250.

[35] T. Sjöstrand, S. Mrenna and P.Z. Skands, *PYTHIA 6.4 Physics and Manual*, *JHEP* **05** (2006) 026 [hep-ph/0603175] [SPIRES].

[36] J. Alwall et al., *MadGraph/MadEvent v4: the new web generation*, *JHEP* **09** (2007) 028 [arXiv:0706.2334] [SPIRES].

[37] P.M. Nadolsky et al., *Implications of CTEQ global analysis for collider observables*, *Phys. Rev.* **D 78** (2008) 013004 [arXiv:0802.0007] [SPIRES].

[38] N. Kidonakis, *Next-to-next-to-leading soft-gluon corrections for the top quark cross section and transverse momentum distribution*, *Phys. Rev.* **D 82** (2010) 114030 [arXiv:1009.4935] [SPIRES].

[39] K. Melnikov and F. Petriello, *Electroweak gauge boson production at hadron colliders through $O(\alpha_s^2)$*, *Phys. Rev.* **D 74** (2006) 114017 [`hep-ph/0609070`] [SPIRES].

[40] CMS collaboration, G.L. Bayatian et al., *CMS technical design report, volume II: Physics performance*, *J. Phys.* **G 34** (2007) 995 [SPIRES].

[41] W. Beenakker, R. Hopker and M. Spira, *PROSPINO: a program for the PROduction of Supersymmetric Particles In Next-to-leading Order QCD*, `hep-ph/9611232` [SPIRES].

[42] CMS collaboration, *Data-driven estimation of the invisible Z background to the SUSY MET plus jets search*, *CMS Physics Analysis Summary* **CMS-PAS-SUS-08-002** (2009).

[43] CMS collaboration, *Isolated photon reconstruction and identification at $\sqrt{s} = 7$ TeV*, *CMS Physics Analysis Summary* **CMS-PAS-EGM-10-006** (2010).

[44] P. Aurenche, M. Fontannaz, J.-P. Guillet, E. Pilon and M. Werlen, *A new critical study of photon production in hadronic collisions*, *Phys. Rev.* **D 73** (2006) 094007 [`hep-ph/0602133`] [SPIRES].

[45] CMS collaboration, V. Khachatryan et al., *Measurement of the isolated prompt photon production cross section in pp collisions at $\sqrt{(s)} = 7$ TeV*, *Phys. Rev. Lett.* **106** (2011) 082001 [`arXiv:1012.0799`] [SPIRES].

[46] Z. Bern et al., *Driving missing data at next-to-leading order*, `arXiv:1106.1423` [SPIRES].

[47] CMS collaboration, V. Khachatryan et al., *Measurements of inclusive W and Z cross sections in pp collisions at $\sqrt{(s)} = 7$ TeV*, *JHEP* **01** (2011) 080 [`arXiv:1012.2466`] [SPIRES].

[48] CMS collaboration, S. Chatrchyan et al., *Measurement of the inclusive Z cross section via decays to tau pairs in pp collisions at $\sqrt{(s)} = 7$ TeV*, submitted to *JHEP* (2011) [`arXiv:1104.1617`] [SPIRES].

[49] CMS collaboration, *Observation of $W \to \tau\nu$ production in pp collisions at $\sqrt{s} = 7$ TeV*, *CMS Physics Analysis Summary* **CMS-PAS-EWK-11-002** (2011).

[50] PARTICLE DATA GROUP collaboration, K. Nakamura et al., *Review of particle physics*, *J. Phys.* **G 37** (2010) 075021 [SPIRES].

[51] B. Efron, *The jackknife, the bootstrap and other resampling plans*, *CBMS-NSF Regional Conference Series in Applied Mathematics* **38**, SIAM, Philadelphia U.S.A. (1982).

[52] CMS collaboration, *Performance of tau reconstruction algorithms in 2010 data collected with CMS*, *CMS Physics Analysis Summary* **CMS-PAS-TAU-11-001** (2011).

[53] CMS collaboration, *Absolute luminosity normalization*, *CMS Detector Performance Summary* **CMS-DP-2011-002** (2011).

[54] F.E. Paige, S.D. Protopopescu, H. Baer and X. Tata, *ISAJET 7.69: a Monte Carlo event generator for pp, $\bar{p}p$ and e^+e^- reactions*, `hep-ph/0312045` [SPIRES].

[55] A.L. Read, *Presentation of search results: The CL(s) technique*, *J. Phys.* **G 28** (2002) 2693 [SPIRES].

[56] T. Junk, *Confidence level computation for combining searches with small statistics*, *Nucl. Instrum. and Meth.* **A 434** (1999) 435.

[57] CMS collaboration, supplemental material added to this publication (2011).

[58] J. Pumplin et al., *New generation of parton distributions with uncertainties from global QCD analysis*, *JHEP* **07** (2002) 012 [`hep-ph/0201195`] [SPIRES].

The CMS collaboration

Yerevan Physics Institute, Yerevan, Armenia

S. Chatrchyan, V. Khachatryan, A.M. Sirunyan, A. Tumasyan

Institut für Hochenergiephysik der OeAW, Wien, Austria

W. Adam, T. Bergauer, M. Dragicevic, J. Erö, C. Fabjan, M. Friedl, R. Frühwirth, V.M. Ghete, J. Hammer[1], S. Hänsel, M. Hoch, N. Hörmann, J. Hrubec, M. Jeitler, W. Kiesenhofer, M. Krammer, D. Liko, I. Mikulec, M. Pernicka, H. Rohringer, R. Schöfbeck, J. Strauss, A. Taurok, F. Teischinger, P. Wagner, W. Waltenberger, G. Walzel, E. Widl, C.-E. Wulz

National Centre for Particle and High Energy Physics, Minsk, Belarus

V. Mossolov, N. Shumeiko, J. Suarez Gonzalez

Universiteit Antwerpen, Antwerpen, Belgium

S. Bansal, L. Benucci, E.A. De Wolf, X. Janssen, J. Maes, T. Maes, L. Mucibello, S. Ochesanu, B. Roland, R. Rougny, M. Selvaggi, H. Van Haevermaet, P. Van Mechelen, N. Van Remortel

Vrije Universiteit Brussel, Brussel, Belgium

F. Blekman, S. Blyweert, J. D'Hondt, O. Devroede, R. Gonzalez Suarez, A. Kalogeropoulos, M. Maes, W. Van Doninck, P. Van Mulders, G.P. Van Onsem, I. Villella

Université Libre de Bruxelles, Bruxelles, Belgium

O. Charaf, B. Clerbaux, G. De Lentdecker, V. Dero, A.P.R. Gay, G.H. Hammad, T. Hreus, P.E. Marage, L. Thomas, C. Vander Velde, P. Vanlaer

Ghent University, Ghent, Belgium

V. Adler, A. Cimmino, S. Costantini, M. Grunewald, B. Klein, J. Lellouch, A. Marinov, J. Mccartin, D. Ryckbosch, F. Thyssen, M. Tytgat, L. Vanelderen, P. Verwilligen, S. Walsh, N. Zaganidis

Université Catholique de Louvain, Louvain-la-Neuve, Belgium

S. Basegmez, G. Bruno, J. Caudron, L. Ceard, E. Cortina Gil, J. De Favereau De Jeneret, C. Delaere[1], D. Favart, A. Giammanco, G. Grégoire, J. Hollar, V. Lemaitre, J. Liao, O. Militaru, C. Nuttens, S. Ovyn, D. Pagano, A. Pin, K. Piotrzkowski, N. Schul

Université de Mons, Mons, Belgium

N. Beliy, T. Caebergs, E. Daubie

Centro Brasileiro de Pesquisas Fisicas, Rio de Janeiro, Brazil

G.A. Alves, L. Brito, D. De Jesus Damiao, M.E. Pol, M.H.G. Souza

Universidade do Estado do Rio de Janeiro, Rio de Janeiro, Brazil

W.L. Aldá Júnior, W. Carvalho, E.M. Da Costa, C. De Oliveira Martins, S. Fonseca De Souza, L. Mundim, H. Nogima, V. Oguri, W.L. Prado Da Silva, A. Santoro, S.M. Silva Do Amaral, A. Sznajder

Instituto de Fisica Teorica, Universidade Estadual Paulista, Sao Paulo, Brazil

C.A. Bernardes[2], F.A. Dias, T.R. Fernandez Perez Tomei, E. M. Gregores[2], C. Lagana, F. Marinho, P.G. Mercadante[2], S.F. Novaes, Sandra S. Padula

Institute for Nuclear Research and Nuclear Energy, Sofia, Bulgaria

N. Darmenov[1], V. Genchev[1], P. Iaydjiev[1], S. Piperov, M. Rodozov, S. Stoykova, G. Sultanov, V. Tcholakov, R. Trayanov

University of Sofia, Sofia, Bulgaria

A. Dimitrov, R. Hadjiiska, A. Karadzhinova, V. Kozhuharov, L. Litov, M. Mateev, B. Pavlov, P. Petkov

Institute of High Energy Physics, Beijing, China

J.G. Bian, G.M. Chen, H.S. Chen, C.H. Jiang, D. Liang, S. Liang, X. Meng, J. Tao, J. Wang, J. Wang, X. Wang, Z. Wang, H. Xiao, M. Xu, J. Zang, Z. Zhang

State Key Lab. of Nucl. Phys. and Tech., Peking University, Beijing, China

Y. Ban, S. Guo, Y. Guo, W. Li, Y. Mao, S.J. Qian, H. Teng, B. Zhu, W. Zou

Universidad de Los Andes, Bogota, Colombia

A. Cabrera, B. Gomez Moreno, A.A. Ocampo Rios, A.F. Osorio Oliveros, J.C. Sanabria

Technical University of Split, Split, Croatia

N. Godinovic, D. Lelas, K. Lelas, R. Plestina[3], D. Polic, I. Puljak

University of Split, Split, Croatia

Z. Antunovic, M. Dzelalija

Institute Rudjer Boskovic, Zagreb, Croatia

V. Brigljevic, S. Duric, K. Kadija, S. Morovic

University of Cyprus, Nicosia, Cyprus

A. Attikis, M. Galanti, J. Mousa, C. Nicolaou, F. Ptochos, P.A. Razis

Charles University, Prague, Czech Republic

M. Finger, M. Finger Jr.

Academy of Scientific Research and Technology of the Arab Republic of Egypt, Egyptian Network of High Energy Physics, Cairo, Egypt

Y. Assran[4], S. Khalil[5], M.A. Mahmoud[6]

National Institute of Chemical Physics and Biophysics, Tallinn, Estonia

A. Hektor, M. Kadastik, M. Müntel, M. Raidal, L. Rebane, A. Tiko

Department of Physics, University of Helsinki, Helsinki, Finland

V. Azzolini, P. Eerola, G. Fedi

Helsinki Institute of Physics, Helsinki, Finland

S. Czellar, J. Härkönen, A. Heikkinen, V. Karimäki, R. Kinnunen, M.J. Kortelainen, T. Lampén, K. Lassila-Perini, S. Lehti, T. Lindén, P. Luukka, T. Mäenpää, E. Tuominen, J. Tuominiemi, E. Tuovinen, D. Ungaro, L. Wendland

Lappeenranta University of Technology, Lappeenranta, Finland

K. Banzuzi, A. Karjalainen, A. Korpela, T. Tuuva

Laboratoire d'Annecy-le-Vieux de Physique des Particules, IN2P3-CNRS, Annecy-le-Vieux, France

D. Sillou

DSM/IRFU, CEA/Saclay, Gif-sur-Yvette, France

M. Besancon, S. Choudhury, M. Dejardin, D. Denegri, B. Fabbro, J.L. Faure, F. Ferri, S. Ganjour, F.X. Gentit, A. Givernaud, P. Gras, G. Hamel de Monchenault, P. Jarry, E. Locci, J. Malcles, M. Marionneau, L. Millischer, J. Rander, A. Rosowsky, I. Shreyber, M. Titov, P. Verrecchia

Laboratoire Leprince-Ringuet, Ecole Polytechnique, IN2P3-CNRS, Palaiseau, France

S. Baffioni, F. Beaudette, L. Benhabib, L. Bianchini, M. Bluj[7], C. Broutin, P. Busson, C. Charlot, T. Dahms, L. Dobrzynski, S. Elgammal, R. Granier de Cassagnac, M. Haguenauer, P. Miné, C. Mironov, C. Ochando, P. Paganini, D. Sabes, R. Salerno, Y. Sirois, C. Thiebaux, B. Wyslouch[8], A. Zabi

Institut Pluridisciplinaire Hubert Curien, Université de Strasbourg, Université de Haute Alsace Mulhouse, CNRS/IN2P3, Strasbourg, France

J.-L. Agram[9], J. Andrea, D. Bloch, D. Bodin, J.-M. Brom, M. Cardaci, E.C. Chabert, C. Collard, E. Conte[9], F. Drouhin[9], C. Ferro, J.-C. Fontaine[9], D. Gelé, U. Goerlach, S. Greder, P. Juillot, M. Karim[9], A.-C. Le Bihan, Y. Mikami, P. Van Hove

Centre de Calcul de l'Institut National de Physique Nucleaire et de Physique des Particules (IN2P3), Villeurbanne, France

F. Fassi, D. Mercier

Université de Lyon, Université Claude Bernard Lyon 1, CNRS-IN2P3, Institut de Physique Nucléaire de Lyon, Villeurbanne, France

C. Baty, S. Beauceron, N. Beaupere, M. Bedjidian, O. Bondu, G. Boudoul, D. Boumediene, H. Brun, J. Chasserat, R. Chierici, D. Contardo, P. Depasse, H. El Mamouni, J. Fay, S. Gascon, B. Ille, T. Kurca, T. Le Grand, M. Lethuillier, L. Mirabito, S. Perries, V. Sordini, S. Tosi, Y. Tschudi, P. Verdier

Institute of High Energy Physics and Informatization, Tbilisi State University, Tbilisi, Georgia

D. Lomidze

RWTH Aachen University, I. Physikalisches Institut, Aachen, Germany

G. Anagnostou, S. Beranek, M. Edelhoff, L. Feld, N. Heracleous, O. Hindrichs, R. Jussen, K. Klein, J. Merz, N. Mohr, A. Ostapchuk, A. Perieanu, F. Raupach, J. Sammet, S. Schael, D. Sprenger, H. Weber, M. Weber, B. Wittmer

RWTH Aachen University, III. Physikalisches Institut A, Aachen, Germany

M. Ata, E. Dietz-Laursonn, M. Erdmann, T. Hebbeker, A. Hinzmann, K. Hoepfner, T. Klimkovich, D. Klingebiel, P. Kreuzer, D. Lanske[†], J. Lingemann, C. Magass, M. Merschmeyer, A. Meyer, P. Papacz, H. Pieta, H. Reithler, S.A. Schmitz, L. Sonnenschein, J. Steggemann, D. Teyssier

RWTH Aachen University, III. Physikalisches Institut B, Aachen, Germany

M. Bontenackels, M. Davids, M. Duda, G. Flügge, H. Geenen, M. Giffels, W. Haj Ahmad, D. Heydhausen, F. Hoehle, B. Kargoll, T. Kress, Y. Kuessel, A. Linn, A. Nowack, L. Perchalla, O. Pooth, J. Rennefeld, P. Sauerland, A. Stahl, M. Thomas, D. Tornier, M.H. Zoeller

Deutsches Elektronen-Synchrotron, Hamburg, Germany

M. Aldaya Martin, W. Behrenhoff, U. Behrens, M. Bergholz[10], A. Bethani, K. Borras, A. Cakir, A. Campbell, E. Castro, D. Dammann, G. Eckerlin, D. Eckstein, A. Flossdorf, G. Flucke, A. Geiser, J. Hauk, H. Jung[1], M. Kasemann, I. Katkov[11], P. Katsas, C. Kleinwort, H. Kluge, A. Knutsson, M. Krämer, D. Krücker, E. Kuznetsova, W. Lange, W. Lohmann[10], R. Mankel, M. Marienfeld, I.-A. Melzer-Pellmann, A.B. Meyer, J. Mnich, A. Mussgiller, J. Olzem, A. Petrukhin, D. Pitzl, A. Raspereza, A. Raval, M. Rosin, R. Schmidt[10], T. Schoerner-Sadenius, N. Sen, A. Spiridonov, M. Stein, J. Tomaszewska, R. Walsh, C. Wissing

University of Hamburg, Hamburg, Germany

C. Autermann, V. Blobel, S. Bobrovskyi, J. Draeger, H. Enderle, U. Gebbert, M. Görner, K. Kaschube, G. Kaussen, H. Kirschenmann, R. Klanner, J. Lange, B. Mura, S. Naumann-Emme, F. Nowak, N. Pietsch, C. Sander, H. Schettler, P. Schleper, E. Schlieckau, M. Schröder, T. Schum, J. Schwandt, H. Stadie, G. Steinbrück, J. Thomsen

Institut für Experimentelle Kernphysik, Karlsruhe, Germany

C. Barth, J. Bauer, J. Berger, V. Buege, T. Chwalek, W. De Boer, A. Dierlamm, G. Dirkes, M. Feindt, J. Gruschke, C. Hackstein, F. Hartmann, M. Heinrich, H. Held, K.H. Hoffmann, S. Honc, J.R. Komaragiri, T. Kuhr, D. Martschei, S. Mueller, Th. Müller, M. Niegel, O. Oberst, A. Oehler, J. Ott, T. Peiffer, G. Quast, K. Rabbertz, F. Ratnikov, N. Ratnikova, M. Renz, C. Saout, A. Scheurer, P. Schieferdecker, F.-P. Schilling, G. Schott, H.J. Simonis, F.M. Stober, D. Troendle, J. Wagner-Kuhr, T. Weiler, M. Zeise, V. Zhukov[11], E.B. Ziebarth

Institute of Nuclear Physics "Demokritos", Aghia Paraskevi, Greece

G. Daskalakis, T. Geralis, S. Kesisoglou, A. Kyriakis, D. Loukas, I. Manolakos, A. Markou, C. Markou, C. Mavrommatis, E. Ntomari, E. Petrakou

University of Athens, Athens, Greece

L. Gouskos, T.J. Mertzimekis, A. Panagiotou, E. Stiliaris

University of Ioánnina, Ioánnina, Greece

I. Evangelou, C. Foudas, P. Kokkas, N. Manthos, I. Papadopoulos, V. Patras, F.A. Triantis

KFKI Research Institute for Particle and Nuclear Physics, Budapest, Hungary

A. Aranyi, G. Bencze, L. Boldizsar, C. Hajdu[1], P. Hidas, D. Horvath[12], A. Kapusi, K. Krajczar[13], F. Sikler[1], G.I. Veres[13], G. Vesztergombi[13]

Institute of Nuclear Research ATOMKI, Debrecen, Hungary

N. Beni, J. Molnar, J. Palinkas, Z. Szillasi, V. Veszpremi

University of Debrecen, Debrecen, Hungary

P. Raics, Z.L. Trocsanyi, B. Ujvari

Panjab University, Chandigarh, India

S.B. Beri, V. Bhatnagar, N. Dhingra, R. Gupta, M. Jindal, M. Kaur, J.M. Kohli, M.Z. Mehta, N. Nishu, L.K. Saini, A. Sharma, A.P. Singh, J. Singh, S.P. Singh

University of Delhi, Delhi, India

S. Ahuja, B.C. Choudhary, P. Gupta, S. Jain, A. Kumar, A. Kumar, M. Naimuddin, K. Ranjan, R.K. Shivpuri

Saha Institute of Nuclear Physics, Kolkata, India

S. Banerjee, S. Bhattacharya, S. Dutta, B. Gomber, S. Jain, R. Khurana, S. Sarkar

Bhabha Atomic Research Centre, Mumbai, India

R.K. Choudhury, D. Dutta, S. Kailas, V. Kumar, P. Mehta, A.K. Mohanty[1], L.M. Pant, P. Shukla

Tata Institute of Fundamental Research - EHEP, Mumbai, India

T. Aziz, M. Guchait[14], A. Gurtu, M. Maity[15], D. Majumder, G. Majumder, K. Mazumdar, G.B. Mohanty, A. Saha, K. Sudhakar, N. Wickramage

Tata Institute of Fundamental Research - HECR, Mumbai, India

S. Banerjee, S. Dugad, N.K. Mondal

Institute for Research and Fundamental Sciences (IPM), Tehran, Iran

H. Arfaei, H. Bakhshiansohi[16], S.M. Etesami, A. Fahim[16], M. Hashemi, A. Jafari[16], M. Khakzad, A. Mohammadi[17], M. Mohammadi Najafabadi, S. Paktinat Mehdiabadi, B. Safarzadeh, M. Zeinali[18]

INFN Sezione di Bari[a], Università di Bari[b], Politecnico di Bari[c], Bari, Italy

M. Abbrescia[a,b], L. Barbone[a,b], C. Calabria[a,b], A. Colaleo[a], D. Creanza[a,c], N. De Filippis[a,c,1], M. De Palma[a,b], L. Fiore[a], G. Iaselli[a,c], L. Lusito[a,b], G. Maggi[a,c], M. Maggi[a], N. Manna[a,b], B. Marangelli[a,b], S. My[a,c], S. Nuzzo[a,b], N. Pacifico[a,b], G.A. Pierro[a], A. Pompili[a,b], G. Pugliese[a,c], F. Romano[a,c], G. Roselli[a,b], G. Selvaggi[a,b], L. Silvestris[a], R. Trentadue[a], S. Tupputi[a,b], G. Zito[a]

INFN Sezione di Bologna[a], Università di Bologna[b], Bologna, Italy

G. Abbiendi[a], A.C. Benvenuti[a], D. Bonacorsi[a], S. Braibant-Giacomelli[a,b], L. Brigliadori[a], P. Capiluppi[a,b], A. Castro[a,b], F.R. Cavallo[a], M. Cuffiani[a,b], G.M. Dallavalle[a], F. Fabbri[a], A. Fanfani[a,b], D. Fasanella[a], P. Giacomelli[a], M. Giunta[a], C. Grandi[a], S. Marcellini[a], G. Masetti[b], M. Meneghelli[a,b], A. Montanari[a], F.L. Navarria[a,b], F. Odorici[a], A. Perrotta[a], F. Primavera[a], A.M. Rossi[a,b], T. Rovelli[a,b], G. Siroli[a,b], R. Travaglini[a,b]

INFN Sezione di Catania[a], Università di Catania[b], Catania, Italy

S. Albergo[a,b], G. Cappello[a,b], M. Chiorboli[a,b,1], S. Costa[a,b], A. Tricomi[a,b], C. Tuve[a,b]

INFN Sezione di Firenze[a], Università di Firenze[b], Firenze, Italy

G. Barbagli[a], V. Ciulli[a,b], C. Civinini[a], R. D'Alessandro[a,b], E. Focardi[a,b], S. Frosali[a,b], E. Gallo[a], S. Gonzi[a,b], P. Lenzi[a,b], M. Meschini[a], S. Paoletti[a], G. Sguazzoni[a], A. Tropiano[a,1]

INFN Laboratori Nazionali di Frascati, Frascati, Italy

L. Benussi, S. Bianco, S. Colafranceschi[19], F. Fabbri, D. Piccolo

INFN Sezione di Genova, Genova, Italy

P. Fabbricatore, R. Musenich

INFN Sezione di Milano-Bicocca^a, Università di Milano-Bicocca^b, Milano, Italy

A. Benaglia^{a,b}, F. De Guio^{a,b,1}, L. Di Matteo^{a,b}, S. Gennai[1], A. Ghezzi^{a,b}, S. Malvezzi^a, A. Martelli^{a,b}, A. Massironi^{a,b}, D. Menasce^a, L. Moroni^a, M. Paganoni^{a,b}, D. Pedrini^a, S. Ragazzi^{a,b}, N. Redaelli^a, S. Sala^a, T. Tabarelli de Fatis^{a,b}

INFN Sezione di Napoli^a, Università di Napoli "Federico II"^{b}, Napoli, Italy

S. Buontempo^a, C.A. Carrillo Montoya^{a,1}, N. Cavallo^{a,20}, A. De Cosa^{a,b}, F. Fabozzi^{a,20}, A.O.M. Iorio^{a,1}, L. Lista^a, M. Merola^{a,b}, P. Paolucci^a

INFN Sezione di Padova^a, Università di Padova^b, Università di Trento (Trento)^c, Padova, Italy

P. Azzi^a, N. Bacchetta^a, P. Bellan^{a,b}, D. Bisello^{a,b}, A. Branca^a, R. Carlin^{a,b}, P. Checchia^a, T. Dorigo^a, U. Dosselli^a, F. Fanzago^a, F. Gasparini^{a,b}, U. Gasparini^{a,b}, A. Gozzelino, S. Lacaprara^{a,21}, I. Lazzizzera^{a,c}, M. Margoni^{a,b}, M. Mazzucato^a, A.T. Meneguzzo^{a,b}, M. Nespolo^{a,1}, L. Perrozzi^{a,1}, N. Pozzobon^{a,b}, P. Ronchese^{a,b}, F. Simonetto^{a,b}, E. Torassa^a, M. Tosi^{a,b}, S. Vanini^{a,b}, P. Zotto^{a,b}, G. Zumerle^{a,b}

INFN Sezione di Pavia^a, Università di Pavia^b, Pavia, Italy

P. Baesso^{a,b}, U. Berzano^a, S.P. Ratti^{a,b}, C. Riccardi^{a,b}, P. Torre^{a,b}, P. Vitulo^{a,b}, C. Viviani^{a,b}

INFN Sezione di Perugia^a, Università di Perugia^b, Perugia, Italy

M. Biasini^{a,b}, G.M. Bilei^a, B. Caponeri^{a,b}, L. Fanò^{a,b}, P. Lariccia^{a,b}, A. Lucaroni^{a,b,1}, G. Mantovani^{a,b}, M. Menichelli^a, A. Nappi^{a,b}, F. Romeo^{a,b}, A. Santocchia^{a,b}, S. Taroni^{a,b,1}, M. Valdata^{a,b}

INFN Sezione di Pisa^a, Università di Pisa^b, Scuola Normale Superiore di Pisa^c, Pisa, Italy

P. Azzurri^{a,c}, G. Bagliesi^a, J. Bernardini^{a,b}, T. Boccali^{a,1}, G. Broccolo^{a,c}, R. Castaldi^a, R.T. D'Agnolo^{a,c}, R. Dell'Orso^a, F. Fiori^{a,b}, L. Foà^{a,c}, A. Giassi^a, A. Kraan^a, F. Ligabue^{a,c}, T. Lomtadze^a, L. Martini^{a,22}, A. Messineo^{a,b}, F. Palla^a, G. Segneri^a, A.T. Serban^a, P. Spagnolo^a, R. Tenchini^a, G. Tonelli^{a,b,1}, A. Venturi^{a,1}, P.G. Verdini^a

INFN Sezione di Roma^a, Università di Roma "La Sapienza"^{b}, Roma, Italy

L. Barone^{a,b}, F. Cavallari^a, D. Del Re^{a,b}, E. Di Marco^{a,b}, M. Diemoz^a, D. Franci^{a,b}, M. Grassi^{a,1}, E. Longo^{a,b}, P. Meridiani, S. Nourbakhsh^a, G. Organtini^{a,b}, F. Pandolfi^{a,b,1}, R. Paramatti^a, S. Rahatlou^{a,b}, C. Rovelli[1]

INFN Sezione di Torino^a, Università di Torino^b, Università del Piemonte Orientale (Novara)^c, Torino, Italy

N. Amapane^{a,b}, R. Arcidiacono^{a,c}, S. Argiro^{a,b}, M. Arneodo^{a,c}, C. Biino^a, C. Botta^{a,b,1}, N. Cartiglia^a, R. Castello^{a,b}, M. Costa^{a,b}, N. Demaria^a, A. Graziano^{a,b,1}, C. Mariotti^a, M. Marone^{a,b}, S. Maselli^a, E. Migliore^{a,b}, G. Mila^{a,b}, V. Monaco^{a,b}, M. Musich^{a,b},

M.M. Obertino^{a,c}, N. Pastrone^a, M. Pelliccioni^{a,b}, A. Potenza^{a,b}, A. Romero^{a,b}, M. Ruspa^{a,c}, R. Sacchi^{a,b}, V. Sola^{a,b}, A. Solano^{a,b}, A. Staiano^a, A. Vilela Pereira^a

INFN Sezione di Trieste^a, Università di Trieste^b, Trieste, Italy

S. Belforte^a, F. Cossutti^a, G. Della Ricca^{a,b}, B. Gobbo^a, D. Montanino^{a,b}, A. Penzo^a

Kangwon National University, Chunchon, Korea

S.G. Heo, S.K. Nam

Kyungpook National University, Daegu, Korea

S. Chang, J. Chung, D.H. Kim, G.N. Kim, J.E. Kim, D.J. Kong, H. Park, S.R. Ro, D. Son, D.C. Son, T. Son

Chonnam National University, Institute for Universe and Elementary Particles, Kwangju, Korea

Zero Kim, J.Y. Kim, S. Song

Korea University, Seoul, Korea

S. Choi, B. Hong, M. Jo, H. Kim, J.H. Kim, T.J. Kim, K.S. Lee, D.H. Moon, S.K. Park, K.S. Sim

University of Seoul, Seoul, Korea

M. Choi, S. Kang, H. Kim, C. Park, I.C. Park, S. Park, G. Ryu

Sungkyunkwan University, Suwon, Korea

Y. Choi, Y.K. Choi, J. Goh, M.S. Kim, J. Lee, S. Lee, H. Seo, I. Yu

Vilnius University, Vilnius, Lithuania

M.J. Bilinskas, I. Grigelionis, M. Janulis, D. Martisiute, P. Petrov, T. Sabonis

Centro de Investigacion y de Estudios Avanzados del IPN, Mexico City, Mexico

H. Castilla-Valdez, E. De La Cruz-Burelo, I. Heredia-de La Cruz, R. Lopez-Fernandez, R. Magaña Villalba, A. Sánchez-Hernández, L.M. Villasenor-Cendejas

Universidad Iberoamericana, Mexico City, Mexico

S. Carrillo Moreno, F. Vazquez Valencia

Benemerita Universidad Autonoma de Puebla, Puebla, Mexico

H.A. Salazar Ibarguen

Universidad Autónoma de San Luis Potosí, San Luis Potosí, Mexico

E. Casimiro Linares, A. Morelos Pineda, M.A. Reyes-Santos

University of Auckland, Auckland, New Zealand

D. Krofcheck, J. Tam

University of Canterbury, Christchurch, New Zealand

P.H. Butler, R. Doesburg, H. Silverwood

National Centre for Physics, Quaid-I-Azam University, Islamabad, Pakistan

M. Ahmad, I. Ahmed, M.I. Asghar, H.R. Hoorani, W.A. Khan, T. Khurshid, S. Qazi

Institute of Experimental Physics, Faculty of Physics, University of Warsaw, Warsaw, Poland

G. Brona, M. Cwiok, W. Dominik, K. Doroba, A. Kalinowski, M. Konecki, J. Krolikowski

Soltan Institute for Nuclear Studies, Warsaw, Poland

T. Frueboes, R. Gokieli, M. Górski, M. Kazana, K. Nawrocki, K. Romanowska-Rybinska, M. Szleper, G. Wrochna, P. Zalewski

Laboratório de Instrumentação e Física Experimental de Partículas, Lisboa, Portugal

N. Almeida, P. Bargassa, A. David, P. Faccioli, P.G. Ferreira Parracho, M. Gallinaro, P. Musella, A. Nayak, J. Pela[1], P.Q. Ribeiro, J. Seixas, J. Varela

Joint Institute for Nuclear Research, Dubna, Russia

S. Afanasiev, P. Bunin, I. Golutvin, V. Karjavin, V. Konoplyanikov, G. Kozlov, A. Lanev, P. Moisenz, V. Palichik, V. Perelygin, M. Savina, S. Shmatov, V. Smirnov, A. Volodko, A. Zarubin

Petersburg Nuclear Physics Institute, Gatchina (St Petersburg), Russia

V. Golovtsov, Y. Ivanov, V. Kim, P. Levchenko, V. Murzin, V. Oreshkin, I. Smirnov, V. Sulimov, L. Uvarov, S. Vavilov, A. Vorobyev, An. Vorobyev

Institute for Nuclear Research, Moscow, Russia

Yu. Andreev, A. Dermenev, S. Gninenko, N. Golubev, M. Kirsanov, N. Krasnikov, V. Matveev, A. Pashenkov, A. Toropin, S. Troitsky

Institute for Theoretical and Experimental Physics, Moscow, Russia

V. Epshteyn, V. Gavrilov, V. Kaftanov[†], M. Kossov[1], A. Krokhotin, N. Lychkovskaya, V. Popov, G. Safronov, S. Semenov, V. Stolin, E. Vlasov, A. Zhokin

Moscow State University, Moscow, Russia

E. Boos, M. Dubinin[23], L. Dudko, A. Ershov, A. Gribushin, O. Kodolova, I. Lokhtin, A. Markina, S. Obraztsov, M. Perfilov, S. Petrushanko, L. Sarycheva, V. Savrin, A. Snigirev

P.N. Lebedev Physical Institute, Moscow, Russia

V. Andreev, M. Azarkin, I. Dremin, M. Kirakosyan, A. Leonidov, S.V. Rusakov, A. Vinogradov

State Research Center of Russian Federation, Institute for High Energy Physics, Protvino, Russia

I. Azhgirey, I. Bayshev, S. Bitioukov, V. Grishin[1], V. Kachanov, D. Konstantinov, A. Korablev, V. Krychkine, V. Petrov, R. Ryutin, A. Sobol, L. Tourtchanovitch, S. Troshin, N. Tyurin, A. Uzunian, A. Volkov

University of Belgrade, Faculty of Physics and Vinca Institute of Nuclear Sciences, Belgrade, Serbia

P. Adzic[24], M. Djordjevic, D. Krpic[24], J. Milosevic

Centro de Investigaciones Energéticas Medioambientales y Tecnológicas (CIEMAT), Madrid, Spain

M. Aguilar-Benitez, J. Alcaraz Maestre, P. Arce, C. Battilana, E. Calvo, M. Cepeda, M. Cerrada, M. Chamizo Llatas, N. Colino, B. De La Cruz, A. Delgado Peris, C. Diez Pardos, D. Domínguez Vázquez, C. Fernandez Bedoya, J.P. Fernández Ramos, A. Ferrando, J. Flix, M.C. Fouz, P. Garcia-Abia, O. Gonzalez Lopez, S. Goy Lopez, J.M. Hernandez, M.I. Josa, G. Merino, J. Puerta Pelayo, I. Redondo, L. Romero, J. Santaolalla, M.S. Soares, C. Willmott

Universidad Autónoma de Madrid, Madrid, Spain

C. Albajar, G. Codispoti, J.F. de Trocóniz

Universidad de Oviedo, Oviedo, Spain

J. Cuevas, J. Fernandez Menendez, S. Folgueras, I. Gonzalez Caballero, L. Lloret Iglesias, J.M. Vizan Garcia

Instituto de Física de Cantabria (IFCA), CSIC-Universidad de Cantabria, Santander, Spain

J.A. Brochero Cifuentes, I.J. Cabrillo, A. Calderon, S.H. Chuang, J. Duarte Campderros, M. Felcini[25], M. Fernandez, G. Gomez, J. Gonzalez Sanchez, C. Jorda, P. Lobelle Pardo, A. Lopez Virto, J. Marco, R. Marco, C. Martinez Rivero, F. Matorras, F.J. Munoz Sanchez, J. Piedra Gomez[26], T. Rodrigo, A.Y. Rodríguez-Marrero, A. Ruiz-Jimeno, L. Scodellaro, M. Sobron Sanudo, I. Vila, R. Vilar Cortabitarte

CERN, European Organization for Nuclear Research, Geneva, Switzerland

D. Abbaneo, E. Auffray, G. Auzinger, P. Baillon, A.H. Ball, D. Barney, A.J. Bell[27], D. Benedetti, C. Bernet[3], W. Bialas, P. Bloch, A. Bocci, S. Bolognesi, M. Bona, H. Breuker, K. Bunkowski, T. Camporesi, G. Cerminara, T. Christiansen, J.A. Coarasa Perez, B. Curé, D. D'Enterria, A. De Roeck, S. Di Guida, N. Dupont-Sagorin, A. Elliott-Peisert, B. Frisch, W. Funk, A. Gaddi, G. Georgiou, H. Gerwig, D. Gigi, K. Gill, D. Giordano, F. Glege, R. Gomez-Reino Garrido, M. Gouzevitch, P. Govoni, S. Gowdy, L. Guiducci, M. Hansen, C. Hartl, J. Harvey, J. Hegeman, B. Hegner, H.F. Hoffmann, A. Honma, V. Innocente, P. Janot, K. Kaadze, E. Karavakis, P. Lecoq, C. Lourenço, T. Mäki, M. Malberti, L. Malgeri, M. Mannelli, L. Masetti, A. Maurisset, F. Meijers, S. Mersi, E. Meschi, R. Moser, M.U. Mozer, M. Mulders, E. Nesvold[1], M. Nguyen, T. Orimoto, L. Orsini, E. Perez, A. Petrilli, A. Pfeiffer, M. Pierini, M. Pimiä, D. Piparo, G. Polese, A. Racz, W. Reece, J. Rodrigues Antunes, G. Rolandi[28], T. Rommerskirchen, M. Rovere, H. Sakulin, C. Schäfer, C. Schwick, I. Segoni, A. Sharma, P. Siegrist, M. Simon, P. Sphicas[29], M. Spiropulu[23], M. Stoye, P. Tropea, A. Tsirou, P. Vichoudis, M. Voutilainen, W.D. Zeuner

Paul Scherrer Institut, Villigen, Switzerland

W. Bertl, K. Deiters, W. Erdmann, K. Gabathuler, R. Horisberger, Q. Ingram, H.C. Kaestli, S. König, D. Kotlinski, U. Langenegger, F. Meier, D. Renker, T. Rohe, J. Sibille[30], A. Starodumov[31]

Institute for Particle Physics, ETH Zurich, Zurich, Switzerland

L. Bäni, P. Bortignon, L. Caminada[32], N. Chanon, Z. Chen, S. Cittolin, G. Dissertori, M. Dittmar, J. Eugster, K. Freudenreich, C. Grab, W. Hintz, P. Lecomte, W. Lustermann, C. Marchica[32], P. Martinez Ruiz del Arbol, P. Milenovic[33], F. Moortgat, C. Nägeli[32], P. Nef, F. Nessi-Tedaldi, L. Pape, F. Pauss, T. Punz, A. Rizzi, F.J. Ronga, M. Rossini, L. Sala, A.K. Sanchez, M.-C. Sawley, B. Stieger, L. Tauscher[†], A. Thea, K. Theofilatos, D. Treille, C. Urscheler, R. Wallny, M. Weber, L. Wehrli, J. Weng

Universität Zürich, Zurich, Switzerland

E. Aguilo, C. Amsler, V. Chiochia, S. De Visscher, C. Favaro, M. Ivova Rikova, B. Millan Mejias, P. Otiougova, C. Regenfus, P. Robmann, A. Schmidt, H. Snoek

National Central University, Chung-Li, Taiwan

Y.H. Chang, K.H. Chen, C.M. Kuo, S.W. Li, W. Lin, Z.K. Liu, Y.J. Lu, D. Mekterovic, R. Volpe, J.H. Wu, S.S. Yu

National Taiwan University (NTU), Taipei, Taiwan

P. Bartalini, P. Chang, Y.H. Chang, Y.W. Chang, Y. Chao, K.F. Chen, W.-S. Hou, Y. Hsiung, K.Y. Kao, Y.J. Lei, R.-S. Lu, J.G. Shiu, Y.M. Tzeng, M. Wang

Cukurova University, Adana, Turkey

A. Adiguzel, M.N. Bakirci[34], S. Cerci[35], C. Dozen, I. Dumanoglu, E. Eskut, S. Girgis, G. Gokbulut, I. Hos, E.E. Kangal, A. Kayis Topaksu, G. Onengut, K. Ozdemir, S. Ozturk[36], A. Polatoz, K. Sogut[37], D. Sunar Cerci[35], B. Tali[35], H. Topakli[34], D. Uzun, L.N. Vergili, M. Vergili

Middle East Technical University, Physics Department, Ankara, Turkey

I.V. Akin, T. Aliev, B. Bilin, S. Bilmis, M. Deniz, H. Gamsizkan, A.M. Guler, K. Ocalan, A. Ozpineci, M. Serin, R. Sever, U.E. Surat, E. Yildirim, M. Zeyrek

Bogazici University, Istanbul, Turkey

M. Deliomeroglu, D. Demir[38], E. Gülmez, B. Isildak, M. Kaya[39], O. Kaya[39], M. Özbek, S. Ozkorucuklu[40], N. Sonmez[41]

National Scientific Center, Kharkov Institute of Physics and Technology, Kharkov, Ukraine

L. Levchuk

University of Bristol, Bristol, United Kingdom

F. Bostock, J.J. Brooke, T.L. Cheng, E. Clement, D. Cussans, R. Frazier, J. Goldstein, M. Grimes, D. Hartley, G.P. Heath, H.F. Heath, L. Kreczko, S. Metson, D.M. Newbold[42], K. Nirunpong, A. Poll, S. Senkin, V.J. Smith

Rutherford Appleton Laboratory, Didcot, United Kingdom

L. Basso[43], K.W. Bell, A. Belyaev[43], C. Brew, R.M. Brown, B. Camanzi, D.J.A. Cockerill, J.A. Coughlan, K. Harder, S. Harper, J. Jackson, B.W. Kennedy, E. Olaiya, D. Petyt, B.C. Radburn-Smith, C.H. Shepherd-Themistocleous, I.R. Tomalin, W.J. Womersley, S.D. Worm

Imperial College, London, United Kingdom

R. Bainbridge, G. Ball, J. Ballin, R. Beuselinck, O. Buchmuller, D. Colling, N. Cripps, M. Cutajar, G. Davies, M. Della Negra, W. Ferguson, J. Fulcher, D. Futyan, A. Gilbert, A. Guneratne Bryer, G. Hall, Z. Hatherell, J. Hays, G. Iles, M. Jarvis, G. Karapostoli, L. Lyons, B.C. MacEvoy, A.-M. Magnan, J. Marrouche, B. Mathias, R. Nandi, J. Nash, A. Nikitenko[31], A. Papageorgiou, M. Pesaresi, K. Petridis, M. Pioppi[44], D.M. Raymond, S. Rogerson, N. Rompotis, A. Rose, M.J. Ryan, C. Seez, P. Sharp, A. Sparrow, A. Tapper, S. Tourneur, M. Vazquez Acosta, T. Virdee, S. Wakefield, N. Wardle, D. Wardrope, T. Whyntie

Brunel University, Uxbridge, United Kingdom

M. Barrett, M. Chadwick, J.E. Cole, P.R. Hobson, A. Khan, P. Kyberd, D. Leslie, W. Martin, I.D. Reid, L. Teodorescu

Baylor University, Waco, USA

K. Hatakeyama, H. Liu

The University of Alabama, Tuscaloosa, USA

C. Henderson

Boston University, Boston, USA

T. Bose, E. Carrera Jarrin, C. Fantasia, A. Heister, J. St. John, P. Lawson, D. Lazic, J. Rohlf, D. Sperka, L. Sulak

Brown University, Providence, USA

A. Avetisyan, S. Bhattacharya, J.P. Chou, D. Cutts, A. Ferapontov, U. Heintz, S. Jabeen, G. Kukartsev, G. Landsberg, M. Luk, M. Narain, D. Nguyen, M. Segala, T. Sinthuprasith, T. Speer, K.V. Tsang

University of California, Davis, Davis, USA

R. Breedon, G. Breto, M. Calderon De La Barca Sanchez, S. Chauhan, M. Chertok, J. Conway, P.T. Cox, J. Dolen, R. Erbacher, E. Friis, W. Ko, A. Kopecky, R. Lander, H. Liu, S. Maruyama, T. Miceli, M. Nikolic, D. Pellett, J. Robles, S. Salur, T. Schwarz, M. Searle, J. Smith, M. Squires, M. Tripathi, R. Vasquez Sierra, C. Veelken

University of California, Los Angeles, Los Angeles, USA

V. Andreev, K. Arisaka, D. Cline, R. Cousins, A. Deisher, J. Duris, S. Erhan, C. Farrell, J. Hauser, M. Ignatenko, C. Jarvis, C. Plager, G. Rakness, P. Schlein[†], J. Tucker, V. Valuev

University of California, Riverside, Riverside, USA

J. Babb, A. Chandra, R. Clare, J. Ellison, J.W. Gary, F. Giordano, G. Hanson, G.Y. Jeng, S.C. Kao, F. Liu, H. Liu, O.R. Long, A. Luthra, H. Nguyen, B.C. Shen[†], R. Stringer, J. Sturdy, S. Sumowidagdo, R. Wilken, S. Wimpenny

University of California, San Diego, La Jolla, USA

W. Andrews, J.G. Branson, G.B. Cerati, D. Evans, F. Golf, A. Holzner, R. Kelley, M. Lebourgeois, J. Letts, B. Mangano, S. Padhi, C. Palmer, G. Petrucciani, H. Pi, M. Pieri, R. Ranieri, M. Sani, V. Sharma, S. Simon, E. Sudano, M. Tadel, Y. Tu, A. Vartak, S. Wasserbaech[45], F. Würthwein, A. Yagil, J. Yoo

University of California, Santa Barbara, Santa Barbara, USA

D. Barge, R. Bellan, C. Campagnari, M. D'Alfonso, T. Danielson, K. Flowers, P. Geffert, J. Incandela, C. Justus, P. Kalavase, S.A. Koay, D. Kovalskyi, V. Krutelyov, S. Lowette, N. Mccoll, V. Pavlunin, F. Rebassoo, J. Ribnik, J. Richman, R. Rossin, D. Stuart, W. To, J.R. Vlimant

California Institute of Technology, Pasadena, USA

A. Apresyan, A. Bornheim, J. Bunn, Y. Chen, M. Gataullin, Y. Ma, A. Mott, H.B. Newman, C. Rogan, K. Shin, V. Timciuc, P. Traczyk, J. Veverka, R. Wilkinson, Y. Yang, R.Y. Zhu

Carnegie Mellon University, Pittsburgh, USA

B. Akgun, R. Carroll, T. Ferguson, Y. Iiyama, D.W. Jang, S.Y. Jun, Y.F. Liu, M. Paulini, J. Russ, H. Vogel, I. Vorobiev

University of Colorado at Boulder, Boulder, USA

J.P. Cumalat, M.E. Dinardo, B.R. Drell, C.J. Edelmaier, W.T. Ford, A. Gaz, B. Heyburn, E. Luiggi Lopez, U. Nauenberg, J.G. Smith, K. Stenson, K.A. Ulmer, S.R. Wagner, S.L. Zang

Cornell University, Ithaca, USA

L. Agostino, J. Alexander, D. Cassel, A. Chatterjee, N. Eggert, L.K. Gibbons, B. Heltsley, W. Hopkins, A. Khukhunaishvili, B. Kreis, G. Nicolas Kaufman, J.R. Patterson, D. Puigh, A. Ryd, M. Saelim, E. Salvati, X. Shi, W. Sun, W.D. Teo, J. Thom, J. Thompson, J. Vaughan, Y. Weng, L. Winstrom, P. Wittich

Fairfield University, Fairfield, USA

A. Biselli, G. Cirino, D. Winn

Fermi National Accelerator Laboratory, Batavia, USA

S. Abdullin, M. Albrow, J. Anderson, G. Apollinari, M. Atac, J.A. Bakken, L.A.T. Bauerdick, A. Beretvas, J. Berryhill, P.C. Bhat, I. Bloch, F. Borcherding, K. Burkett, J.N. Butler, V. Chetluru, H.W.K. Cheung, F. Chlebana, S. Cihangir, W. Cooper, D.P. Eartly, V.D. Elvira, S. Esen, I. Fisk, J. Freeman, Y. Gao, E. Gottschalk, D. Green, K. Gunthoti, O. Gutsche, J. Hanlon, R.M. Harris, J. Hirschauer, B. Hooberman, H. Jensen, M. Johnson, U. Joshi, R. Khatiwada, B. Klima, K. Kousouris, S. Kunori, S. Kwan, C. Leonidopoulos, P. Limon, D. Lincoln, R. Lipton, J. Lykken, K. Maeshima, J.M. Marraffino, D. Mason, P. McBride, T. Miao, K. Mishra, S. Mrenna, Y. Musienko[46], C. Newman-Holmes, V. O'Dell, R. Pordes, O. Prokofyev, N. Saoulidou, E. Sexton-Kennedy, S. Sharma, W.J. Spalding, L. Spiegel, P. Tan, L. Taylor, S. Tkaczyk, L. Uplegger, E.W. Vaandering, R. Vidal, J. Whitmore, W. Wu, F. Yang, F. Yumiceva, J.C. Yun

University of Florida, Gainesville, USA

D. Acosta, P. Avery, D. Bourilkov, M. Chen, S. Das, M. De Gruttola, G.P. Di Giovanni, D. Dobur, A. Drozdetskiy, R.D. Field, M. Fisher, Y. Fu, I.K. Furic, J. Gartner, B. Kim, J. Konigsberg, A. Korytov, A. Kropivnitskaya, T. Kypreos, K. Matchev, G. Mitselmakher, L. Muniz, C. Prescott, R. Remington, A. Rinkevicius, M. Schmitt, B. Scurlock, P. Sellers, N. Skhirtladze, M. Snowball, D. Wang, J. Yelton, M. Zakaria

Florida International University, Miami, USA

V. Gaultney, L. Kramer, L.M. Lebolo, S. Linn, P. Markowitz, G. Martinez, J.L. Rodriguez

Florida State University, Tallahassee, USA

T. Adams, A. Askew, J. Bochenek, J. Chen, B. Diamond, S.V. Gleyzer, J. Haas, S. Hagopian, V. Hagopian, M. Jenkins, K.F. Johnson, H. Prosper, L. Quertenmont, S. Sekmen, V. Veeraraghavan

Florida Institute of Technology, Melbourne, USA

M.M. Baarmand, B. Dorney, S. Guragain, M. Hohlmann, H. Kalakhety, R. Ralich, I. Vodopiyanov

University of Illinois at Chicago (UIC), Chicago, USA

M.R. Adams, I.M. Anghel, L. Apanasevich, Y. Bai, V.E. Bazterra, R.R. Betts, J. Callner, R. Cavanaugh, C. Dragoiu, L. Gauthier, C.E. Gerber, D.J. Hofman, S. Khalatyan, G.J. Kunde[47], F. Lacroix, M. Malek, C. O'Brien, C. Silkworth, C. Silvestre, A. Smoron, D. Strom, N. Varelas

The University of Iowa, Iowa City, USA

U. Akgun, E.A. Albayrak, B. Bilki, W. Clarida, F. Duru, C.K. Lae, E. McCliment, J.-P. Merlo, H. Mermerkaya[48], A. Mestvirishvili, A. Moeller, J. Nachtman, C.R. Newsom, E. Norbeck, J. Olson, Y. Onel, F. Ozok, S. Sen, J. Wetzel, T. Yetkin, K. Yi

Johns Hopkins University, Baltimore, USA

B.A. Barnett, B. Blumenfeld, A. Bonato, C. Eskew, D. Fehling, G. Giurgiu, A.V. Gritsan, Z.J. Guo, G. Hu, P. Maksimovic, S. Rappoccio, M. Swartz, N.V. Tran, A. Whitbeck

The University of Kansas, Lawrence, USA

P. Baringer, A. Bean, G. Benelli, O. Grachov, R.P. Kenny Iii, M. Murray, D. Noonan, S. Sanders, J.S. Wood, V. Zhukova

Kansas State University, Manhattan, USA

A.F. Barfuss, T. Bolton, I. Chakaberia, A. Ivanov, S. Khalil, M. Makouski, Y. Maravin, S. Shrestha, I. Svintradze, Z. Wan

Lawrence Livermore National Laboratory, Livermore, USA

J. Gronberg, D. Lange, D. Wright

University of Maryland, College Park, USA

A. Baden, M. Boutemeur, S.C. Eno, D. Ferencek, J.A. Gomez, N.J. Hadley, R.G. Kellogg, M. Kirn, Y. Lu, A.C. Mignerey, K. Rossato, P. Rumerio, F. Santanastasio, A. Skuja, J. Temple, M.B. Tonjes, S.C. Tonwar, E. Twedt

Massachusetts Institute of Technology, Cambridge, USA

B. Alver, G. Bauer, J. Bendavid, W. Busza, E. Butz, I.A. Cali, M. Chan, V. Dutta, P. Everaerts, G. Gomez Ceballos, M. Goncharov, K.A. Hahn, P. Harris, Y. Kim, M. Klute, Y.-J. Lee, W. Li, C. Loizides, P.D. Luckey, T. Ma, S. Nahn, C. Paus, D. Ralph, C. Roland, G. Roland, M. Rudolph, G.S.F. Stephans, F. Stöckli, K. Sumorok, K. Sung, E.A. Wenger, R. Wolf, S. Xie, M. Yang, Y. Yilmaz, A.S. Yoon, M. Zanetti

University of Minnesota, Minneapolis, USA

S.I. Cooper, P. Cushman, B. Dahmes, A. De Benedetti, P.R. Dudero, G. Franzoni, J. Haupt, K. Klapoetke, Y. Kubota, J. Mans, N. Pastika, V. Rekovic, R. Rusack, M. Sasseville, A. Singovsky, N. Tambe

University of Mississippi, University, USA

L.M. Cremaldi, R. Godang, R. Kroeger, L. Perera, R. Rahmat, D.A. Sanders, D. Summers

University of Nebraska-Lincoln, Lincoln, USA

K. Bloom, S. Bose, J. Butt, D.R. Claes, A. Dominguez, M. Eads, J. Keller, T. Kelly, I. Kravchenko, J. Lazo-Flores, H. Malbouisson, S. Malik, G.R. Snow

State University of New York at Buffalo, Buffalo, USA

U. Baur, A. Godshalk, I. Iashvili, S. Jain, A. Kharchilava, A. Kumar, S.P. Shipkowski, K. Smith, J. Zennamo

Northeastern University, Boston, USA

G. Alverson, E. Barberis, D. Baumgartel, O. Boeriu, M. Chasco, S. Reucroft, J. Swain, D. Trocino, D. Wood, J. Zhang

Northwestern University, Evanston, USA

A. Anastassov, A. Kubik, N. Odell, R.A. Ofierzynski, B. Pollack, A. Pozdnyakov, M. Schmitt, S. Stoynev, M. Velasco, S. Won

University of Notre Dame, Notre Dame, USA

L. Antonelli, D. Berry, A. Brinkerhoff, M. Hildreth, C. Jessop, D.J. Karmgard, J. Kolb, T. Kolberg, K. Lannon, W. Luo, S. Lynch, N. Marinelli, D.M. Morse, T. Pearson, R. Ruchti, J. Slaunwhite, N. Valls, M. Wayne, J. Ziegler

The Ohio State University, Columbus, USA

B. Bylsma, L.S. Durkin, J. Gu, C. Hill, P. Killewald, K. Kotov, T.Y. Ling, M. Rodenburg, G. Williams

Princeton University, Princeton, USA

N. Adam, E. Berry, P. Elmer, D. Gerbaudo, V. Halyo, P. Hebda, A. Hunt, J. Jones, E. Laird, D. Lopes Pegna, D. Marlow, T. Medvedeva, M. Mooney, J. Olsen, P. Piroué, X. Quan, B. Safdi, H. Saka, D. Stickland, C. Tully, J.S. Werner, A. Zuranski

University of Puerto Rico, Mayaguez, USA

J.G. Acosta, X.T. Huang, A. Lopez, H. Mendez, S. Oliveros, J.E. Ramirez Vargas, A. Zatserklyaniy

Purdue University, West Lafayette, USA

E. Alagoz, V.E. Barnes, G. Bolla, L. Borrello, D. Bortoletto, M. De Mattia, A. Everett, A.F. Garfinkel, L. Gutay, Z. Hu, M. Jones, O. Koybasi, M. Kress, A.T. Laasanen, N. Leonardo, C. Liu, V. Maroussov, P. Merkel, D.H. Miller, N. Neumeister, I. Shipsey, D. Silvers, A. Svyatkovskiy, H.D. Yoo, J. Zablocki, Y. Zheng

Purdue University Calumet, Hammond, USA

P. Jindal, N. Parashar

Rice University, Houston, USA

C. Boulahouache, K.M. Ecklund, F.J.M. Geurts, B.P. Padley, R. Redjimi, J. Roberts, J. Zabel

University of Rochester, Rochester, USA

B. Betchart, A. Bodek, Y.S. Chung, R. Covarelli, P. de Barbaro, R. Demina, Y. Eshaq, H. Flacher, A. Garcia-Bellido, P. Goldenzweig, Y. Gotra, J. Han, A. Harel, D.C. Miner, D. Orbaker, G. Petrillo, W. Sakumoto, D. Vishnevskiy, M. Zielinski

The Rockefeller University, New York, USA

A. Bhatti, R. Ciesielski, L. Demortier, K. Goulianos, G. Lungu, S. Malik, C. Mesropian

Rutgers, the State University of New Jersey, Piscataway, USA

O. Atramentov, A. Barker, D. Duggan, Y. Gershtein, R. Gray, E. Halkiadakis, D. Hidas, D. Hits, A. Lath, S. Panwalkar, R. Patel, K. Rose, S. Schnetzer, S. Somalwar, R. Stone, S. Thomas

University of Tennessee, Knoxville, USA

G. Cerizza, M. Hollingsworth, S. Spanier, Z.C. Yang, A. York

Texas A&M University, College Station, USA

R. Eusebi, W. Flanagan, J. Gilmore, A. Gurrola, T. Kamon, V. Khotilovich, R. Montalvo, I. Osipenkov, Y. Pakhotin, J. Pivarski, A. Safonov, S. Sengupta, A. Tatarinov, D. Toback, M. Weinberger

Texas Tech University, Lubbock, USA

N. Akchurin, C. Bardak, J. Damgov, C. Jeong, K. Kovitanggoon, S.W. Lee, T. Libeiro, P. Mane, Y. Roh, A. Sill, I. Volobouev, R. Wigmans, E. Yazgan

Vanderbilt University, Nashville, USA

E. Appelt, E. Brownson, D. Engh, C. Florez, W. Gabella, M. Issah, W. Johns, P. Kurt, C. Maguire, A. Melo, P. Sheldon, B. Snook, S. Tuo, J. Velkovska

University of Virginia, Charlottesville, USA

M.W. Arenton, M. Balazs, S. Boutle, B. Cox, B. Francis, R. Hirosky, A. Ledovskoy, C. Lin, C. Neu, R. Yohay

Wayne State University, Detroit, USA

S. Gollapinni, R. Harr, P.E. Karchin, P. Lamichhane, M. Mattson, C. Milstène, A. Sakharov

University of Wisconsin, Madison, USA

M. Anderson, M. Bachtis, J.N. Bellinger, D. Carlsmith, S. Dasu, J. Efron, L. Gray, K.S. Grogg, M. Grothe, R. Hall-Wilton, M. Herndon, A. Hervé, P. Klabbers, J. Klukas, A. Lanaro, C. Lazaridis, J. Leonard, R. Loveless, A. Mohapatra, F. Palmonari, D. Reeder, I. Ross, A. Savin, W.H. Smith, J. Swanson, M. Weinberg

†: Deceased

1: Also at CERN, European Organization for Nuclear Research, Geneva, Switzerland

2: Also at Universidade Federal do ABC, Santo Andre, Brazil

3: Also at Laboratoire Leprince-Ringuet, Ecole Polytechnique, IN2P3-CNRS, Palaiseau, France

4: Also at Suez Canal University, Suez, Egypt

5: Also at British University, Cairo, Egypt

6: Also at Fayoum University, El-Fayoum, Egypt

7: Also at Soltan Institute for Nuclear Studies, Warsaw, Poland

8: Also at Massachusetts Institute of Technology, Cambridge, USA

9: Also at Université de Haute-Alsace, Mulhouse, France

10: Also at Brandenburg University of Technology, Cottbus, Germany

11: Also at Moscow State University, Moscow, Russia

12: Also at Institute of Nuclear Research ATOMKI, Debrecen, Hungary

13: Also at Eötvös Loránd University, Budapest, Hungary

14: Also at Tata Institute of Fundamental Research - HECR, Mumbai, India

15: Also at University of Visva-Bharati, Santiniketan, India

16: Also at Sharif University of Technology, Tehran, Iran

17: Also at Shiraz University, Shiraz, Iran

18: Also at Isfahan University of Technology, Isfahan, Iran

19: Also at Facoltà Ingegneria Università di Roma ”La Sapienza”, Roma, Italy

20: Also at Università della Basilicata, Potenza, Italy

21: Also at Laboratori Nazionali di Legnaro dell’ INFN, Legnaro, Italy

22: Also at Università degli studi di Siena, Siena, Italy

23: Also at California Institute of Technology, Pasadena, USA

24: Also at Faculty of Physics of University of Belgrade, Belgrade, Serbia

25: Also at University of California, Los Angeles, Los Angeles, USA

26: Also at University of Florida, Gainesville, USA

27: Also at Université de Genève, Geneva, Switzerland

28: Also at Scuola Normale e Sezione dell’ INFN, Pisa, Italy

29: Also at University of Athens, Athens, Greece

30: Also at The University of Kansas, Lawrence, USA

31: Also at Institute for Theoretical and Experimental Physics, Moscow, Russia

32: Also at Paul Scherrer Institut, Villigen, Switzerland

33: Also at University of Belgrade, Faculty of Physics and Vinca Institute of Nuclear Sciences, Belgrade, Serbia

34: Also at Gaziosmanpasa University, Tokat, Turkey

35: Also at Adiyaman University, Adiyaman, Turkey

36: Also at The University of Iowa, Iowa City, USA

37: Also at Mersin University, Mersin, Turkey

38: Also at Izmir Institute of Technology, Izmir, Turkey

39: Also at Kafkas University, Kars, Turkey

40: Also at Suleyman Demirel University, Isparta, Turkey

41: Also at Ege University, Izmir, Turkey

42: Also at Rutherford Appleton Laboratory, Didcot, United Kingdom

43: Also at School of Physics and Astronomy, University of Southampton, Southampton, United Kingdom

44: Also at INFN Sezione di Perugia; Università di Perugia, Perugia, Italy

45: Also at Utah Valley University, Orem, USA

46: Also at Institute for Nuclear Research, Moscow, Russia

47: Also at Los Alamos National Laboratory, Los Alamos, USA

48: Also at Erzincan University, Erzincan, Turkey